Glia mediated ionic balance in the stem cell niche is required for the proper proliferation of neurogenic tissues and wiring of neural circuits.

Haritz Plazaola-Sasieta[1], Qi Zhu[1], Héctor Gaitán-Peñas[2,3], Martín Rios[1], Raúl Estévez[2,3], Marta Morey[1,4 *]

[1]Departament de Genètica, Microbiologia i Estadística, Facultat de Biologia, Universitat de Barcelona, Barcelona, Spain;

[2]Departament de Ciencies Fisiològiques, Genes Disease and Therapy Program IDIBELL-Institute of Neurosciences, Universitat de Barcelona, L'Hospitalet de Llobregat, Spain;

[3]Centro de Investigación Biomédica en Red de Enfermedades Raras (CIBERER), Instituto de Salud Carlos III, Madrid, Spain

[4]Institut de Biomedicina de la Universitat de Barcelona (IBUB), Barcelona, Spain

* Corresponding Author

ABSTRACT

The cellular niche that surrounds stem cells modulates their self-renewal and proliferative properties. In the nervous system glial cells form part of the neural stem cell niche and express a wide variety of ion channels. While the physiological roles of ion channels in glia have been mainly studied in the mature nervous system, the contribution of glial ion channel function in the niche to nervous system development is poorly understood. To gain insight we explored the function of the *Drosophila ClC-a* chloride channel since its human ortholog *CLCN2* is expressed in glial cells and impairment of its function results in neurodevelopmental disorders. We found *ClC-a* expressed in the niche in cortex glia. These glial cells are in close association with neurogenic tissues and also wrap neuronal cell bodies as they mature away from the niche. Characterization of loss of function *ClC-a* mutants showed these animals had smaller brains and widespread axon guidance defects. Here we show that *ClC-a* is required in cortex glia for the proliferation of neuroepithelial cells and neuroblasts, as well as for neuronal survival. We could also relate the axon guidance defects observed in photoreceptors to impaired proliferation in a neuroblast lineage that generates guidepost glial cells essential for this process. Taken together, our results show that ion channels expressed in glia forming part of the neural stem cell niche can have a significant impact on nervous system development. We propose that ion channels can non-autonomously modulate the number of neural progenitors and the progeny of neuroblast lineages, consequently affecting the correct assembly of neural circuits.

INTRODUCTION

Stem cells remarkable proliferative capacity needs to be tightly regulated to ensure the generation of the appropriate amount of cells during development or tissue homeostasis in adulthood. This regulation is controlled in part by stem cell intrinsic programs, but also extrinsic cues provided by the cellular niche that surrounds them. In the nervous system of both vertebrates and invertebrates, glia form part of the niche for neural stem/progenitor cells (Bjornsson et al., 2015; Ruddy and Morshead, 2018). In both systems, the effect of glia on neurogenic tissues has been mainly related to the secretion of factors that regulate the maintenance, proliferation and differentiation of stem and progenitor cells. However, one of the findings that shattered the view of glia as just a passive structural element was the realization that glial cells expressed a large variety of ion channels and neurotransmitter receptors (Barres, 1991; Barres et al., 1990). While physiological roles for several of these ion channels in glia have emerged both in normal and pathological states of the mature nervous system (Black and Waxman, 2013; Nwaobi et al., 2016; Olsen et al., 2015; Pappalardo et al., 2016; Verkhrastsky and Steinhauser, 2000), the contribution of glial ion channel functions specifically in the niche during nervous system development is poorly understood. To address this issue and given the functional parallelisms between vertebrate and *Drosophila* glia (Chotard and Salecker, 2004; Corty and Freeman, 2013; Freeman and Doherty, 2006), we turned to the fly, where neurogenesis has been extensively studied and the niche is simpler than in vertebrates.

The fly central nervous system contains three structures: the central brain (CB), the ventral nerve cord (VNC) and the optic lobe (OL). The CB and VNC are generated by neural stem cells called neuroblasts that delaminate from the neuroectodem during

embryonic development and give rise to larval and adult brain through two rounds of neurogenesis (Doe, 2008). The OL originates from a group of neuroepithelial cells that proliferates and separates into two crescent shaped primordia, the outer and the inner proliferation centers (OPC and IPC), which will produce NBs and precursor cells of the distinct visual processing centers (Apitz and Salecker, 2014). In addition, the OL has been extensively used as a model to address neural circuit assembly (Plazaola-Sasieta et al., 2017). This is mainly because of the modular nature of the fly eye and its stereotyped development, which allow for an easy detection of wiring defects in photoreceptors and other visual system neurons.

The cellular components in the fly niche are the neurogenic cells themselves (neuroepithelia and/or NBs and precursor cells), the newly generated neurons and three types of glia. Among the niche glia, perineural and subperineural glia are components of the blood brain barrier (BBB) that respond to systemic nutritional cues and signal neuroblasts to proliferate (Chell and Brand, 2010; Kanai et al., 2018; Perez-Gomez et al., 2013; Sousa-Nunes et al., 2011; Spéder and Brand, 2014). Cortex glia are large cells that lay below subperineural glia. Both nutritional cues and neuroblast signals induce the remodeling of cortex glia to encase NBs and their immediate progeny in a chamber and older neurons individually (Read, 2018; Spéder and Brand, 2018). This close association protects NBs from oxidative stress and nutritional restriction (Bailey et al., 2015; Cheng et al., 2011), and is essential for neuronal survival (Coutinho-Budd et al., 2017; Dumstrei et al., 2003; Pereanu et al., 2005; Read, 2018; Spéder and Brand, 2018). In the OL, a distinct subtype of cortex glia that expresses miRNA mir-8 (surface associated cortex glia) is in direct contact with the OPC (Morante et al., 2013). This glia sends signals that regulate the expansion of the neuroepithelium and the timely

neuroepithelium to neuroblast transition (Morante et al., 2013). Connectivity is also influenced by glia in the visual system (Chotard and Salecker, 2008; Poeck et al., 2001). Indeed different types of glial cells control photoreceptor axon pathfinding from the eye to the brain and the targeting of a subset of photoreceptors to the lamina neuropil.

The vertebrate ClC-2 chloride channel has been proposed to be one of the channels involved in K^+ buffering, a key ionic homeostasis process in which glia are involved (Jentsch and Pusch, 2018). In the mature nervous system, increased neural activity results in an increase of extracellular K^+, which can alter neuronal excitability. To lower down the concentration of K^+, astrocytes take up the ion and distribute it to distant sites via the astrocytic syncytia. The intake of K^+ takes place with the concomitant intake of Cl^- and water, producing transient astrocyte swelling (Bellot-Saez et al., 2017). Based on its expression in astrocytic glia, the ClC-2 channel has been proposed to be one of the channels that could participate in this Cl^- uptake (Blanz et al., 2007; Hoegg-Beiler et al., 2014; Sirisi et al., 2017). Mutations in *CLCN2* are causative for Leukoencephalopathy with ataxia (LKPAT) (Depienne et al., 2013) and ClC-2 has been related to Megalencephalic leukoencephalopathy with subcortical cysts (MLC) (Hoegg-Beiler et al., 2014; Jeworutzki et al., 2012; Sirisi et al., 2017). Both conditions are characterized by vacuolization of the white matter and edema, most probably a consequence of impaired K^+ buffering, but in addition patients can also present learning disabilities and mild to moderate mental retardation. The fact that ClC-2 is expressed during development in glial precursors, is required for their differentiation (Hou et al., 2018) and that intellectual impairment can arise from connectivity defects, suggest that this channel could have additional functions during neural development.

To test this possibility we focused on ClC-a, the fly homolog of the vertebrate ClC-2 chloride channel (Wang et al., 2017). ClC-a electrophysiological properties have been described and are very similar to its mammalian counterpart (Flores et al., 2009; Jeworutzki et al., 2012). In addition, both ClC-2 and ClC-a are most abundant in epitheliums and the brain. ClC-2 has been shown to play a role in transepithelial transport in enterocytes (Catalán et al., 2004). Similarly, ClC-a is also expressed in the epithelia of the fly digestive system, and it is involved in transepithelial transport in stellate cells of the Malpighian tubules, the fly secretory system (Cabrero et al., 2014; Denholm et al., 2013). In the vertebrate brain, in addition to glia, ClC-2 is expressed in inhibitory neurons where it regulates neuronal excitability (Földy et al., 2010; Ratte and Prescott, 2011; Rinke et al., 2010). We were interested in the observation that *ClC-a* mRNA is expressed in the developing fly nervous system already at embryonic stages in glia (Kearney et al., 2004; Tomancak et al., 2007, 2002) and highly expressed throughout development of the nervous system (Celniker et al., 2009; Rose et al., 2007), which indicated a possible role of the channel in the development of the nervous system.

In this study we have analyzed the expression pattern of *Drosophila ClC-a* in the brain, characterized the first loss of function mutant alleles of this chloride channel and investigated their effects on the development of the nervous system. We show that *ClC-a* is expressed in several types of glia and uncovered a role for this channel in the niche. It's expression in cortex glia, which is in close contact with OPC and IPC neuroepithelial cells and NBs, is necessary for the proper mitotic activity of these neurogenic tissues, as well as for the survival of neurons. One of the secondary consequences of reduced neuroblast proliferation was the significantly limited

production of guidepost glial cells, which translated into non-autonomous neural circuit assembly phenotypes in photoreceptors. Both neurogenic and connectivity defects could be rescued by glial specific expression of the rat ClC-2 vertebrate channel. We propose that the expression of ion channels in the glial niche can shape the development of the nervous system, both controlling the number of neurons generated as well as and their connectivity.

RESULTS

ClC-a is expressed in two types of glia in the developing brain: cortex glia and ensheathing glia.

To characterize in detail *ClC-a* expression in the developing brain at different larval stages (L1, L2 and L3) we used reporter lines and antibodies. One of these reporter lines expresses GAL4 under the *ClC-a* endogenous regulatory sequences (see later in the text) and it recapitulates the *ClC-a* expression pattern in Malpighian tubule stellate cells observed with an antibody against ClC-a (this study and Cabrero et al., 2014) and a ClC-a protein trap (*ClC-a-GFP*) (Supplementary Information and Supplementary Figure 1A-C). To visualize and follow *ClC-a* expressing cells along development we combined the *ClC-a-GAL4* line with UAS transgenes that outlined the membrane and labeled the nucleus. *ClC-a* expression was detected in L1 brains on membranes in contact with the developing OPC neuroepithelium (Figure 1A, B). Colocalization of the nuclear RFP signal with the pan glial nuclear marker Repo indicated that *ClC-a* was expressed in a subset of glial cells (Figure 1A, A'). In L2 brains glial membranes started encasing CB neuroblasts (Figure 1C), and more membrane processes were observed deeper in the brain (Figure 1D). By late L3 the number of ClC-a^{+} glial nucleus in the CB had greatly increased and their glial membranes confined neuroblasts and their

lineages in chambers (Figure 1E). A slightly deeper section showed ClC-a$^+$ glial processes forming a smaller mesh (Figure 1F) which ensheaths mature neurons. In the OL, the OPC and IPC, which were still producing neuroblasts and progenitors, continued to be surrounded by ClC-a$^+$ glial membranes (Figure 1G). We also noticed a glial process between the developing lamina (i.e. lamina precursor cells or LPC) and the lobula plug (LoP) (Figure 1H), establishing a boundary between these two regions which are innervated by neurons with different origins (i.e. photoreceptors generated in the eye disc and innervating the OL through the LPC area and distal neurons generated from the d-IPC, a region of the IPC) (Figure 1I). Similar expression patterns were observed with anti-ClC-a antibodies and the ClC-a protein trap, confirming the specificity of the *ClC-a-GAL4* driver line in the brain (Supplementary Figure 1D-I).

We next aimed to identify which types of glial cells expressed *ClC-a* and for that we used cell type specific markers and nuclei position. We concluded that superficial ClC-a$^+$ nuclei on top of the OPC neuroepithelium correspond to a subtype of cortex glia called surface associated cortex glia (Morante et al., 2013), which lies below perineural and subperineural glia (Figure 1J). miRNA *mir-8* (Karres et al., 2007)), a marker for this subtype of cortex glia (Morante et al., 2013), colocalized with ClC-a protein in cells covering the OPC and the process separating the LPC from the LoP (Figure 1K). Additional experiments indicated that ClC-a$^+$ nuclei present on the surface of the CB and in cortical areas belong to cortex glia. The membrane and nuclear patterns of *ClC-a*$^+$ cells were consistent with the nuclear patterns and the membrane scaffold, also known as trophospongium (Hoyle et al., 1986), observed with the recently described cortex glia driver *wrapper* (Coutinho-Budd et al., 2017) (compare Figure 1G with Figure 1L). As a matter of fact, there was extensive colocalization between *ClC-a*$^+$ and

wrapper^{+} membranes in the CB and OL (Figure 1M-N), including surface associated cortex glia over the OPC (Figure 1N, N”). Thus, for simplicity, we will refer to surface associated cortex glia as cortex glia.

In order to assess the presence of glial types other than cortex glia, we used an intersectional strategy whereby only *ClC-a*$^{+}$*/wrapper*$^{-}$ cells (i.e. non-cortex glia cells) were labeled. This way we identified that *ClC-a* was also expressed in different subtypes of ensheathing glia such as neuropil- and tract-ensheathing glia. *ClC-a* was expressed in neuropil ensheathing glia surrounding CB neuropils, including the mushroom body calix (Figure 1O, P). For tract-ensheathing glia *ClC-a* was expressed in glia around the mushroom body peduncle (Figure 1O), and in the OL in the outer (Xg_o) (Figure 1Q) and inner (Xg_i) (Supplementary Figure 2E-G) chiasm glia, cell types that wrap axonal tracts between the lamina and medulla, and medulla and lobula complex respectively. A detailed developmental analysis revealed expression in other glial cells in the OL as well as in the VNC and peripheral nervous system (Supplementary Figure 2). Most of the *ClC-a*$^{+}$ glial types observed in the late L3 stage still appeared labeled in the adult (Supplementary Figure 2G).

Taken together these data indicate that *ClC-a* is expressed already early on in development in cortex glia cells, which are in direct contact with and wrap proliferative tissues such as the neuroepithelia of the OL (OPC, IPC) and neuroblasts in the CB, forming part of the niche. *ClC-a* is also expressed in different types of ensheathing glia whose processes contribute to the compartmentalization of the brain by demarcating different neuropils and neuronal tracts.

MiMIC insertions in the *ClC-a* locus generate strong loss of function alleles.

To explore the role of *ClC-a* in glia we set out to characterize a set of *Minos*-mediated integration cassette (Mi(MIC)) insertions into the *ClC-a* locus (Figure 2A). This transposon contains a gene trap cassette that results in the formation of truncated transcripts (Venken et al., 2011) (Figure 2B). We focused on *Mi(MIC)ClC-a*^{05423} and *Mi(MIC)ClC-a*^{14007} alleles (from now own referred to as *05423* and *14007*), since their insertion sites were predicted to interrupt all isoforms of the *ClC-a* gene. The *ClC-a-GAL4* line we have used was derived from *Mi(MIC)ClC-a*^{05423} by the Gene Disruption Project (Nagarkar-Jaiswal et al., 2015a, 2015b) by recombinase-mediated cassette exchange (RMCE) replacement of the MiMIC gene trap cassette for a GAL4 cassette (Diao et al., 2015) (Figure 2B). Hence, a mutant allele is generated that expresses GAL4 under the control of *ClC-a* regulatory sequences. From now on we will refer to it as *05423*$^{ClC\text{-}a\text{-}GAL4}$. Initial viability characterization of these insertions over deficiency *Df(3R)PS2* (*Df*) revealed the presence of escapers (Supplementary Information). Through genetic and mutant phenotype analyses (Supplementary Information and Figure 2G) allelic combinations can be ordered by strength in the following sequence: *05423*$^{ClC\text{-}a\text{-}GAL4}$*/Df* > *05423/Df* > *14007/Df* = *05423*$^{ClC\text{-}a\text{-}GAL4}$*/14007* > *05423/14007* > *14007/14007*. Since it is difficult to obtain *05423*$^{ClC\text{-}a\text{-}GAL4/}$*Df* or *05423/Df* animals in enough numbers, we have mainly used *14007/Df* and *05423*$^{ClC\text{-}a\text{-}GAL4}$*/14007* flies in our experiments. Indeed, these two allelic combinations behave in a very similar fashion, and represent a good compromise in terms of phenotypic strength and mutant animal availability. In addition, the *05423*$^{ClC\text{-}a\text{-}GAL4}$*/14007* combination allows for the visualization in the mutant background of the glial cells that express ClC-a in the wild type situation.

The predicted loss of function nature of the MiMIC insertions characterized was confirmed by immunostaining and western blot. The *ClC-a* expression pattern observed with anti-ClC-a antibody in wild type L3 stellate cells of the Malpighian tubules and brains was not detected in any of the mutant allelic combinations tested (Supplementary Figure 3A-D). Western blots revealed that with very low frequency the splice machinery used the endogenous splice acceptor instead of the MiMIC one, and that, although extremely low, there was a remnant of wild type protein in mutants only detectable in immunoblots (Supplementary Figure 3E).

In summary, here we have characterized the first *ClC-a* mutant alleles and found them to result in strong loss of function of the gene product.

Mutations in *ClC-a* result in smaller brains with photoreceptor guidance defects.

To address the effect of *ClC-a* mutations in brain development we started by dissecting adult brains and searching for defects that could have a developmental origin based on *ClC-a* expression patterns in the larval brain. The observation that *ClC-a* was expressed in glia over proliferative tissues in the brain (i.e. neuroepithelia and neuroblasts) led us to hypothesize that mutant brains could be smaller than control ones, and to test this idea we measured OLs from control and mutant animals. We indeed observed a reduction in OL size in mutants particularly evident in $05423^{ClC\text{-}a\text{-}GAL4}/Df$, the strongest allelic combination, and also present in the $05423^{ClC\text{-}a\text{-}GAL4}/14007$ (Figure 2C) and *14007/Df* (Figure 4H, I).

Given that we detected *ClC-a* expression in glial processes separating the developing lamina from the LoP and outer chiasm glial cells, we labeled photoreceptors to assess

their innervation path. The compound eye of the fly is formed by some 800 units called ommatidia. Each ommatidia contains eight photoreceptors, R1-6 that terminate in the lamina forming the lamina plexus, and R7 and R8 that extend to the medulla. As rows of ommatidia form in the eye disc, photoreceptors extend axons and innervate the OL in a sequential manner. This way a retinotopic map forms and each ommatidia in the eye generates a corresponding processing unit in the lamina and the medulla neuropils. This is particularly well reflected by the ordered array of R7 and R8 photoreceptor axons in the medulla, where defects in wiring can be detected easily. In control adult OLs (Figure 2E schematic), R-cell axons from the posterior edge of the eye, enter through the posterior lamina where R1-6 stop. R7 and R8 axons traverse the outer optic chiasm, and project into the anterior-most medulla; similarly, R-cell axons from the anterior region of the eye project into the posterior medulla. All R7 and R8 axons enter the medulla neuropil from its distal face and their projections align in a stereotyped array forming a retinotopic map (Figure 2E).

Analysis of *ClC-a* mutant adult OLs using a pan photoreceptor marker revealed photoreceptor guidance defects. The guidance phenotypes observed could be classified into three levels of severity based on the proportion of R cell axons affected (Figure 2F). In brains with phenotypes classified as medium, a significant portion of posterior R cell axons bypassed the outer chiasm, projected along the posterior edge of the medulla neuropil turning anteriorly, and extended for variable distances before innervating the medulla neuropil from its proximal face. In many cases this resulted in the lamina neuropil being posteriorly misplaced. Despite the presence of these discreet bundles of misprojected axons that originate posteriorly, the photoreceptor array was maintained and mostly regular. We classified as weak phenotypes instances of few misprojected

posterior axons. Strong phenotypes were characterized by a severe disruption of the photoreceptor array and a posteriorly located and disorganized lamina. Despite the difficulty of identifying discreet bundles of photoreceptor axons, distal innervation was evident. The penetrance and expressivity of these three degrees of severity was variable depending on the allelic combination analyzed (Figure 2G). This variability could be explained by the fact that *ClC-a* mutants were not complete nulls. Detailed analysis of mutant photoreceptors also revealed layer selection defects for R8 and R1-R6 neurons (Supplementary Figure 4A-J).

In order to confirm the requirement of *ClC-a* in glia we performed cell type specific knock down and rescue experiments. In addition to the *ClC-a* driver, we also used the general glial driver Repo-GAL4 as an alternative to restrict transgene expression selectively to glia. Using these two drivers the knock down of *ClC-a* by RNAi phenocopied the photoreceptor phenotypes seen in the mutant (Figure 2H). Moreover, the expression with both glial drivers of *ClC-a* and rat *CLCN2* cDNA, rescued the photoreceptor phenotypes in whole mutant animals, as well as their developmental delay (Figure 2I). Although it has been suggested that pupal photoreceptors express *ClC-a* (Ugarte et al., 2005), we did not observe it with antibodies (data not shown) or reporters used in this study, neither in larval nor pupal or adults stages (Supplementary Figure 2D-G). In addition, the absence of phenotype when knocking down *ClC-a* in the eye disc or generating a full eye mutant for *ClC-a* (EGUF-hid approach, data not shown), together with the inability to rescue the guidance phenotype when expressing *ClC-a* in photoreceptors (Supplementary Figure 4K), confirmed that *ClC-a* was required in glia for photoreceptor guidance.

Remarkably, taking advantage of the *05423*$^{ClC\text{-}a\text{-}GAL4}$ allele we observed a rescue of both the OL size and photoreceptor guidance phenotypes in *05423*$^{ClC\text{-}a\text{-}GAL4}$*/Df*, the strongest allelic combination, with both *ClC-a* and *ClCN2* cDNA transgenes (Figure 2D, I). This result indicated that both the brain size reduction and photoreceptor guidance phenotypes in *ClC-a* mutants are non-autonomous, dependent on the chloride channel expression in glia and that the fly and rat channel have equivalent functions.

Expression of *ClC-a* in cortex glia is required for neuroepithelial expansion and neuroblast divisions, and sufficient to restore brain size.

Aiming to unravel how mutations in *ClC-a* resulted in smaller brains we first assessed the status of glia in *ClC-a* mutants. We used the *05423*$^{ClC\text{-}a\text{-}GAL4}$*/14007* allelic combination to visualize the membranes and nucleus of glia in the mutant background. Our analysis showed that the distribution pattern of glial cell bodies on the surface of the brain and deep in the cortex was similar in control and mutant animals. Although the ratio of number of nuclei/hemisphere volume in the mutant was slightly reduced compared to control (Supplementary Figure 5A), importantly, the membrane scaffold looked indistinguishable from the one observed in controls covering the whole hemisphere. Processes of *ClC-a* mutant cortex glia were in close contact with the OPC and IPC neuroepithelia just like in control animals (Figure 3A, B, E, F). In addition, both in the OL and the CB cortex glia processes formed the trophospongium. That is individual neuroblasts were enclosed in chambers that enlarged to adapt to their lineage expansion (Figure 3C, G), and mature neuronal cell bodies were progressively enwrapped by cortex glia processes (Figure 3D, D’, H, H’). From these observations we conclude that mutations in the channel do not result in major morphological changes of the trophospongium formed by cortex glia.

In turn, these results suggested that *ClC-a* was instead required for the proper physiology of cortex glia. Cortex glia has been shown to be essential for neurogenesis (Dumstrei et al., 2003), and since cortex glia processes are tightly associated to the OPC (surface associated cortex glia (Morante et al., 2013)) and IPC, we set out to examine whether the small OLs in mutant adult brain (Figure 2C) were a consequence of defects in these neuroepithelia. Neuroepithelia in the OL start as sheets of cells that divide symmetrically and expand until mid L3 (Ngo et al., 2010). As they do so, they bend along the dorso-ventral axis resulting in a crescent shape structure with the opening pointing posteriorly (Nassif et al., 2003). Already in late L2, while the OPC still grows to expand the pool of prospective neuroblasts, neuroepithelium to neuroblast transition starts taking place. The lateral edge gives rise to LPC and the medial edge to neuroblasts that will produce medulla neurons and glia (Egger et al., 2007, 2010; Ngo et al., 2010; Orihara-Ono et al., 2011; Reddy et al., 2010; Wang et al., 2011a, 2011b; Weng et al., 2012; Yasugi et al., 2010, 2008). Once neuroepithelium divisions stop and the wave of differentiation continues, the OPC will start reducing in size and disappear in early pupal stages when it is all converted into precursors and neuroblasts. A similar process takes place in the IPC where different domains generate neuroblasts or migrating progenitors (Apitz and Salecker, 2015; Hofbauer and Campos-Ortega, 1990) until the neuroepithelium disappears.

We first checked if there were differences in neuroepithelia between control and mutant animals. For this we stained brains with the neuroepithelium marker E-cadherin and manually segmented the tissue to generate a 3D reconstruction of these structures, which gave us information about their morphology (Figure 4A) and size (Figure 4B). In

control animals in the mid L3 stage, the OPC and IPC crescents had their ends close together. In late L3, with the addition of progeny from neuroblasts, the OL was bigger and neuroepithelia crescents wider and thinner. In comparison, in mid L3 mutant animals, while neuroepithelia had the same crescent shape as in controls they were already clearly smaller (Figure 4B). By late L3, in most cases, the OPC appeared as two separate dorsal and ventral domains with the central part absent. Similarly, part of the IPC was also missing (Figure 4A).

We next wondered whether the reduction in the size of the neuroepithelial sheets was due to cell death and to test that we stained larval brains with an antibody against the apoptosis marker Dcp-1 (cleaved death caspase protein-1). Although developmental cell death was taking place generally in the brain, we did not observe apoptotic cells neither in control nor mutant neuroepithelial cells in mid or late L3 stages (Figure 4C). Thus, the absence of cell death in this tissue suggested that defects in proliferation could be the cause for the reduction in size of the OPC and IPC at mid L3, as well as the morphological defects in late L3. The lack of neuroepithelial cells in the OPC central domain could be due differentiation taking place (Supplementary Figure 6) in a neuroepithelium with reduced proliferation hence resulting in a premature disappearance of the tissue. To address proliferation defects we carried out a clonal analysis study. With this technique, once mitotic recombination is induced in a dividing neuroepithelial cell, its progeny is labeled, and thus can be counted. Clones were generated in the L2 stage while the neuroepithelia are dividing and expanding, and their size assessed 48 hours later at mid L3. Neuroepithelia clones generated in the control background (brains where cortex glia expressed the ClC-a channel) had a median size of 21 cells for OPC clones and 14,5 cells for IPC clones. Conversely, clones generated in

the mutant background (brains where cortex glia did not express *ClC-a*) were significantly reduced with a median size of 9 and 8 cells for OPC and IPC clones respectively (Figure 4D). Thus, *ClC-a* was necessary in cortex glia for neuroepithelial expansion.

Given that *ClC-a* expressing cortex glia also covers the neuroblasts that originate from the OPC as well as the neuroblasts in the CB we also used clonal analysis to assess neuroblast divisions in *ClC-a* mutants. The high density and proximity of neuroblasts originating from the OPC makes it difficult to obtain single neuroblasts clones sufficiently apart of each other to be sure that the labeled progeny belongs to a single neuroblast. Thus, we analyzed proliferation in neuroblasts from the CB since they are sufficiently apart from each other. Importantly, both control and mutant animals had the same number of neuroblasts, so CB size reduction in mutants was not due to a decrease in neuroblasts (Supplementary Figure 5B). Using the same clone induction protocol as for neuroepithelial clones, the median size of type I neuroblast clones in the control background was 34 cells, while for clones in the mutant brackground the median size was reduced to 26 cells (Figure 4E). At this same mid L3 stage we also detected that outside neuroepithelia, which were death free, there was more cell death in mutant than control brains (Figure 4F). This result suggested that alterations in the physiology of cortex glia in *ClC-a* mutants affected the trophic role of cortex glia processes that wrap the cell bodies of the more mature neurons of the lineage (Coutinho-Budd et al., 2017; Dumstrei et al., 2003; Pereanu et al., 2005; Read, 2018; Spéder and Brand, 2018). Thus we cannot discard that the reduction in neuroblast clone size could be a combination of both cell death and proliferation defects.

Taken together, these data argue that the lack of *ClC-a* in cortex glia in the niche affects the proliferation of neuroepithelial cells and neuroblasts, as well as for the viability of mature neurons that receive trophic signals from cortex glia. Indeed, consistent with both these observations the size and growth rate of larval hemispheres was reduced in the mutant background (Figure 4G). Thus, these results are in accordance with both OL (Figure 4H) and CB (Figure 4I) of adult *ClC-a* mutant brains being smaller than those of control flies. Importantly, in addition, expression of *ClC-a* exclusively in cortex glia was sufficient to rescue the size of both structures in the adult (Figure 4J, K).

Defects are also observed in the neuroblast lineage that gives rise to ClC-a$^+$ ensheathing glia, which are necessary guideposts for photoreceptor axons innervating the medulla.

In an attempt to understand how the non-autonomous photoreceptor guidance phenotype related to *ClC-a* expression in the OL, we performed a detailed developmental expression analysis in the region where photoreceptor innervation takes place. In control L2 brains, horizontal views showed the OPC and IPC still juxtaposed and *ClC-a*$^+$ cell bodies on the surface of the brain and in the CB (Figure 1D). In L3 frontal views we observed that a population of glia, which preceded the arrival of photoreceptors axons in the lamina (Dearborn, 2004; Perez and Steller, 1996), progressively positioned amid the expanding region between the OPC and IPC during the early to mid L3 stages (Figure 5A, B). This population was divided in two sets of nuclei, the *ClC-a*$^-$ nuclei of satellite glia (Supplementary Figure 8A, B) and a population of *ClC-a*$^+$ nucleus, with lower expression than cortex glia, which we called boundary glia (Figure 5B). From this seemingly homogenous mid L3 boundary glia population, in late L3 brains two cell types could be distinguished in frontal (Figure 5C) and

horizontal views (Figure 5D, Supplementary Figure 8C): the Xg_o and a glial type that had never been described before. We called these cells palisade glia (pag) and they positioned in the same plane as the cortex glia projection and the Xg_o forming a continuous glial barrier between the developing lamina and the LoP. We do not know if pag reach to or which type they are in the adult (Figure 5E). Xg_o is considered tract ensheating glia and one glial cell enwraps an average of 15 lamina-medulla fiber tracts (Kremer et al., 2017). Two independent studies have shown that Xg_o, as well as Xg_i, originate from the type II DL1 neuroblast lineage and migrate to the OL (Ren et al., 2018; Viktorin et al., 2013). We repeated DL1 lineage-tracing experiments and observed that progeny from the DL1 populated the OL following the same temporal pattern as ClC-a^+ boundary glia (Supplementary Figure 8D-F). Hence, our data supports the idea that boundary glia are DL1 progeny that will differentiate into the newly described pag and Xg_o. Quantification of boundary glia in control brains showed how their numbers increased from early to mid L3 and then dropped at late L3 (Figure 5M, Supplementary Figure 8 G, H). In mutant brains, however, we observed a striking reduction in the number of boundary glia cells in mid and late L3 stages (Figure 5G-J, M). Given that no glial apoptosis was observed in the region (Supplementary Figure 8I, J), this result indicated that just very few boundary glia reached the OL in *ClC-a* mutants.

To study the cause of this strong reduction we first used the *earmuff* R09D11 genomic enhancer-fragment driven reporter CD4-tdtomato (Han et al., 2011) to selectively label all type II neuroblast lineages and assess DL1. Type II neuroblast lineages are characterized by the generation of intermediate neural progenitors (INP) that can undergo several rounds of additional asymmetric divisions before they disappear

(Boone and Doe, 2008). In control brains there are 8 type II neuroblasts, 6 positioned medially (DM1-6) and 2 laterally (DL1/2) closer to the OL (Figure 5N, O). In mutants, although we observed some brains with instances of DM mispositioning, DL1/2 cluster could be found together and laterally located with respect to the rest of DM neuroblasts (Figure 5P, Q). However, their position with respect to the OL was sometimes changed. To assess proliferation defects in the lineage our initial approach was to compare control to mutant DL1 clones. However, even though the clonal analysis protocol used in our study was very similar to those used in other studies where they analyzed type II clones, which are identified by the presence of INPs (Dpn positive cells in the lineage), we hardly obtained any type II clones (2 out of 116 analyzed clones) and none in the DL1/2 cluster. As an alternative, we reasoned that we could use the number of INPs in a lineage as readout for proliferation (Figure 5R). Since DL1 and DL2 secondary axon tracts are extremely similar, we differentiated the two lineages by the expression of *gcm-LacZ* in the DL2 lineage (Viktorin et al., 2013) (Supplementary Figure 9A), which consistently contained less INPs than DL1 (Supplementary Figure 9B). The comparison between control and mutant revealed that both DL1 and DL2 lineages contained a higher number of INPs in the mutant condition (Figure 5S-U). Given that we have also observed proliferation defects in neuroepithelial sheets and neuroblasts, it is reasonable to suggest that one of the causes for the strong reduction in boundary glia in mutants could be a reduced proliferation of DL1 INPs and hence their accumulation. In addition to defects in proliferation, it is formally possible that defects in migration also contribute to the strong reduction of boundary glia in mutant OLs. The fact that the DL1/2 cluster could be found at different relative positions with respect to the OL, and that the IPC, which is the region where these cells enter the OL in normal conditions, is

defective in mutants could result in boundary glia having difficulties to reach their final destination.

At this point the question of how did the strong reduction of boundary glia affect photoreceptor guidance arose. Given that the presence of boundary glia in mid L3 coincides with the beginning of photoreceptor innervation we next addressed the spatiotemporal relationship between these two cell types in control flies. As rows of ommatidia form in the eye disc, photoreceptors extend axons that reach the OL through the optic stalk. In mid L3 stages, R8s from the first rows of ommatida projected into the posterior part of the field of LPC and their axons were found very close to boundary glia as they continued to the medulla (Figure 6A, B). Photoreceptor innervation coincided with cellular rearrangements, where boundary glia start to separate into pag and Xg_o glia. Thus, in slightly older brains R1-6 axons stopped and formed the lamina plexus above the boundary glia cells that will become Xg_o, R8 axons traversed the outer optic chiasm passing by very close to the Xg_o (Figure 6C, D) and continued to the medulla innervating it through its distal face (Figure 5F). Thus, photoreceptors are in close proximity to pag and $Xg_{o.}$ Conversely, in mutant brains the strong reduction in boundary glia, and consequently Xg_o, resulted in posterior R8 axons skipping the outer chiasm and innervating the medulla from its proximal face (Figure 5L). The severity of the initial photoreceptor guidance errors determined the strength of the adult guidance phenotypes. Consistent with *ClC-a* expression in Xg_o and Xg_i, the malformation of chiasms in *ClC-a* mutants results in the altered positioning of OL neuropils in the adult brain (compare Figure 5E with Figure 5K).

Both the developmental guidance defects and the adult outcomes of *ClC-a* mutants are extremely similar to OL specific *slit* mutants (Figure 6E-H) and *robo3* mutants (Pappu et al., 2011; Tayler et al., 2004). The secreted chemorepellent molecule Slit and the Robo family of receptors (Robo, Robo2, Robo3) have been indeed implicated in preventing the mixing of photoreceptor axons with the axons of distal neurons from the LoP during development, and hence maintaining the compartmentalization of that region of the developing brain (Tayler et al., 2004). While receptors have been shown to be required in neurons, *slit* reporters suggested that Slit protein in the region could be contributed by Xg_o (Pappu et al., 2011; Tayler et al., 2004). The detailed developmental analysis on the assembly of the glial barrier allowed us to unequivocally characterize the *slit* temporal and cellular expression pattern with respect to photoreceptor innervation. To this end we characterized and used a MiMIC-based protein trap line for Slit (Supplementary Information, Supplementary Figure 10). Our analysis indicated that Slit was already expressed in boundary glia in mid L3 (Figure 6I-K) when photoreceptors innervate the brain and their axons come in close proximity with these glial cells. Moreover, removal of one copy of *slit* enhanced the *ClC-a* photoreceptor guidance phenotype suggesting a genetic interaction between these two genes (Figure 6L), and knocking down *slit* in *ClC-a*$^+$ glia in the barrier recapitulated the photoreceptor guidance defects (Figure 6M).

Taking into consideration our results and previously published studies (Fan et al., 2005; Pappu et al., 2011; Suzuki et al., 2016; Tayler et al., 2004), we propose that the substantial reduction in boundary glia is most probably a combination of proliferation and migration defects, which results in a significant reduction in Slit protein in the region. As a consequence, photoreceptors that innervate the OL close to the glial

boundary fasciculate with the axons of neurons in the LoP known to innervate the medulla from its proximal site.

Expression of *ClC-a* exclusively in cortex glia is sufficient to restore ensheathing glia guidepost cells and rescue photoreceptor guidance defects.

To formally test that *ClC-a* was sufficient in cortex glia to regulate DL1 proliferation, and assess if *ClC-a* expression in boundary glia (cell type classified as ensheathing glia) played any role in photoreceptor guidance, we performed a cell type specific rescue experiment. Because there is no reporter described exclusively labeling boundary glia before photoreceptor innervation, we carried out a cortex glia specific rescue. We reasoned that with a cortex glia specific driver we would rescue the generation of boundary glia from DL1 and at the same time avoid ClC-a expression in boundary glia (Figure 7A). Since in this experiment we could not label boundary glia specifically, we used Repo to mark and count glial nucleus in the region in mid L3, when the first photoreceptors begin to innervate the brain. At this time the glial population is compact and easy to identify, while in late L3 additional ClC-a^{-} glia such as epithelial and marginal glia appear in high numbers and complicate the counting. In control animals, mid L3 glia nuclei included ClC-a^{-} satellite glia and boundary glia (Figure 7A, B). While in mutants the number of glial cells is reduced to half due to the strong reduction of boundary glial cells (Figure 7A, B), expression of *ClC-a* exclusively in cortex glia resulted in an almost complete rescue in the number of glial cells present in the barrier region in mid L3 (Figure 7A, B). More importantly, this boundary glia rescue resulted in the rescue of the photoreceptor guidance phenotype (Figure 7C). Surprisingly, the autonomous *ClC-a* expression in boundary glia is not necessary for their viability, for migration from their point of origin in the CB to position themselves in the OL, and for

Slit secretion, since photoreceptor guidance defects are fully rescued when boundary glia are in their position but do not express *ClC-a*. Thus, we conclude that the absence of boundary glia and the photoreceptor guidance phenotypes are a secondary consequence of the *ClC-a* requirement in cortex glia and its function in neuroblast proliferation.

Mutations in *ClC-a* result in widespread wiring defects.

While we have characterized the origin of the guidance defects seen in photoreceptors, wiring defects are not restricted to this cell type. The position and morphology of neuropils in the visual system of *ClC-a* animals indicate that the wiring of many other neurons in this system is probably affected as well (compare Figure 5E to K). Moreover, we have also observed defects in CB structures such as mushroom bodies (MBs). Each hemisphere contains one MB, which is formed by the neurons derived from four special type I neuroblasts that never enter quiescence. These neurons extend dendrites forming the calyx and axons project in a fascicle called the peduncle that splits into two branches called lobes (Figure 8A). Similar to photoreceptors, mushroom bodies are neural structures highly dependent on glia-neuron interactions. It has been shown that glia wrap the peduncle and the lobes during development (Spindler et al., 2009) and in the adult (Kremer et al., 2017), and that different type II DM neuroblasts contribute glia that associates with the mushroom body (Ren et al., 2018). In control animals, ClC-a^{+} glia surrounded the MB calyx (Figure 8B) and the peduncle (Figure 8D). Newly differentiated neurons, which are FasII^{-}, projected their axons through the center of the peduncle generating in a ring-like FasII^{+} pattern labeling the oldest neurons (Figure 8C). In *ClC-a* mutant animals, in many cases axons misprojected to the calyx (Figure 8F) and FasII staining filled in the center of the peduncle suggesting that

newly generated axons did not project through the center of this structure (Figure 8G). In addition, the peduncle was much thinner (Figure 8G) although it seemed that there still was ClC-a$^+$ glia surrounding it. Comparison of control and mutant brains stained with antibody against N-cadherin, which labels neuropils, showed how the calyx, which in controls appeared deep in the brain (Figure 8E), was more superficial in mutants (Figure 8I). MB clones (Figure 8J) confirmed defects in the calyx and the peduncle (compare Figure8K to M and O). In MB clones in the control background, axons from the clone stayed together in a bundle and extended into the center of the peduncle (Figure 8L). In instances where MB clones in the mutant background extended axons to the peduncle (Figure 8M), these axons defasciculated and projected to the peduncle through its periphery leaving older axons in the center (Figure 8N). In clones with strong phenotypes almost all axons terminated in the calyx and the peduncle was barely visible (Figure 8M). Interestingly, these defects are very similar to those observed when cortex glia and neuropile glia are eliminated: abnormal mushroom body morphologies including splaying of axons and misguidance, and misshapen superficial calix due to premature fusion of the four MB lineages in the cortical region (Spindler et al., 2009). Thus, as we have observed for photoreceptor guidance phenotypes, the MB defects in *ClC-a* mutants could arise due to a reduced production of glia, ClC-a$^+$ or otherwise, associated to mushroom body circuitry. In summary then, since guidance defects in the *ClC-a* mutant seem to be widespread, we propose that *ClC-a* requirement for proper circuit assembly is not restricted to the OL but general to the brain.

DISCUSSION

In this study we show that the *ClC-a* chloride channel function in the glial niche has a non-autonomous but profound effect on two key aspects of neural development: the

generation of neurons and glia in the appropriate numbers, time and place through its role in regulating the proliferation of neurogenic tissues; and as a consequence, the correct assembly of neural circuits. Importantly, the fact that the fly (ClC-a) and rat (ClC-2) chloride channels rescue brain size and guidance defects, suggests that both can perform the same physiological function. Concomitant defects in neuroblast proliferation and photoreceptor targeting have been observed in other studies (González et al., 1989; Kanai et al., 2018; Zhu et al., 2008) and the Activin signaling pathway has been proposed to be required for the production of the proper number of neurons to enable proper connection of incoming photoreceptors axons to their targets (Zhu et al., 2008). Interestingly, mutations in the proneural gene *asense*, which is expressed in type I neuroblasts and INPs, has adult targeting phenotypes extremely similar to the ones observed in *ClC-a* mutants (González et al., 1989). Along the same line, our work links *ClC-a* photoreceptor guidance phenotypes to INP proliferation defects, and moreover, identifies the INP-derived cellular population required for proper photoreceptor axon guidance.

In addition to leukoencephalopathy, patients with mutations in *CLCN2* display pathologies associated to cognitive defects. *CLCN2* mutant mice also develop widespread vacuolization that progresses with age, but besides photoreceptor and male germ cell degeneration, they do not display immediately visible behavioral defects (Blanz et al., 2007; Bösl et al., 2001; Edwards et al., 2010). However, the fact that *CLCN2* is expressed in astrocytes and oligodendrocytes early in development (Makara et al., 2003), and that it has been detected in Bergman glia (Jeworutzki et al., 2012), which is important for neuronal migration in the formation of cortical structures, suggest that it would be worth exploring the role the channel could be playing in

nervous system development. Moreover, interestingly, expression of *CLCN2* has been found outside the brain in an unrelated stem cell niche. *CLCN2* is expressed in Sertoli cells, which are the primary somatic cells of the seminiferous epithelium that form the spermatogonial stem cell niche through physical support and expression of paracrine factors (Chen et al., 2005; Oatley et al., 2011). *CLCN2* mutant mice showed disorganized distribution of germ cells in tubules at 3 weeks, germ cells did not pass beyond meiosis I and were completely lost at later stages (Bösl et al., 2001; Edwards et al., 2010). Hence, in a parallel way as ClC-a regulates proliferation in the neural stem cell niche, ClC-2 could be regulating proliferation in the spermatogonial stem cell niche.

While the Sertoli *CLCN2* expression/germ cell depletion correlation in mouse is in accordance with our data suggesting an important role of the ClC-a/ClC-2 chloride channel in stem cell niches, how a chloride ion channel could non-autonomously modulate the mitotic activity of proliferative cells remains to be elucidated. One of the possibilities we considered was whether ionic imbalance in *ClC-a* mutants affected secretion. Glial cells secrete different types of factors to the extracellular space both for the maintenance of their morphology in the adult and during development (Coutinho-Budd et al., 2017; Read, 2018; Spéder and Brand, 2018). In the niche in particular there are several examples of glia secreted molecules that regulate proliferation such as the transforming growth factor a (TGF-a)-like ligand (Morante et al., 2013), insulin like peptides (dILPs) (Chell and Brand, 2010; Sousa-Nunes et al., 2011). In vertebrates, elevation in intracellular Ca^{2+} in astrocytes, caused by the activation of G protein–coupled receptors and release of calcium from intracellular stores or calcium entry from the extracellular space through different types of channels, has been reported to evoke

the release of gliotransmitters (Bazargani and Attwell, 2016; Khakh and McCarthy, 2015; Shigetomi et al., 2016). To test the possibility that *ClC-a/ClCN2* regulated secretion we performed RNAi knock down of key upstream regulators of intracellular calcium release, *Drosophila* IP3R and RyR receptors, and downstream effectors of calcium-regulated secretory vesicle exocytosis, as well as secretion assays in primary glial cultures where *ClCN2* was knocked down with RNAi (data not shown). However, we were not able to consistently recapitulate *ClC-a* mutant phenotypes or detect secretion defects, suggesting that if the absence or reduction of the channel impairs secretion it does so only in a very limited way.

Another possibility is that ClC-a is involved in pH regulation. Under extracellular neutral pH, H^+ and HCO_3^- combine to form H_2CO_3, which is in turn is in equilibrium with H_2O and CO_2. In acidic conditions, to compensate the increase in H^+, the HCO_3^- /Cl^- exchangers extrude HCO_3^- to the extracellular space to form more H_2CO_3 and push the reaction to the formation of H_2O and CO_2. Rat ClC-2 opens in response to extracellular acidification allowing Cl^- to exit the cell (Jordt and Jentsch, 1997). Since for each molecule of HCO_3^- extruded one of Cl^- is internalized, ClC-2 activation might be required to regulate HCO_3^- transport allowing for the presence of extracellular Cl^- and this way creating a Cl^- recycling pathway for HCO_3^-/Cl^- exchangers (Bösl et al., 2001). Assays in *Xenopus* oocytes concluded that ClC-a activity is also sensitive to pH (H. G-P and R. E unpublished results). Thus, it could be that the lack of ClC-a in cortex glia would lead to a more acidic extracellular pH, due to deficient Cl^- recycling for HCO_3^-/Cl^- exchangers. Since changes in extracellular and intracellular pH have been shown to affect the proliferative capacity of both wild type and cancer cells (Carswell and Papoutsakis, 2000; Ciapa and Philippe, 2013; Flinck et al., 2018; Persi et al., 2018;

White et al., 2017), ClC-a function in pH regulation could explain the proliferation defects observed in the mutant.

Regardless of the molecular mechanism that mediates ClC-a effect on proliferation our findings contribute to the notion that glia mediated ionic balance is important for brain development. Our findings are in accordance with recent studies suggesting a link between ion channels and the development of the nervous system, with channels being important both in stem cells (Li, 2011; Liebau et al., 2013) as well as glia (Olsen et al., 2015). A recent example of a channel function in stem cells is the gene SCN3A, which codes for NaV1.3 sodium channel. This channel is expressed mostly during development and highly enriched in the basal/outer radial glia progenitors and migrating newborn neurons (Smith et al., 2018). The appearance of this type of progenitors and defined neuronal migration has been associated to the establishment of gyri in the cortex (Fietz et al., 2010; Hansen et al., 2010; Reillo et al., 2011). Intriguingly, mutations in the SCN3A gene result in structural malformations of gyri in the cortex (Smith et al., 2018). Another example is the glia specific Kir 4.1 channel, which is related to neurodevelopmental disorders with associated cognitive defects. Mutations in *KCNJ10*, which codes for the glial specific Kir4.1 channel, underlie SeSAME/EAST Syndrome (Seizures, Sensorineural deafness, Ataxia, Mental retardation and Electrolyte imbalance/Epilepsy, Ataxia, Sensorineural deafness and Tubulopathy) (Bockenhauer et al., 2009; Scholl et al., 2009) and have been detected in patients diagnosed with autism spectrum disorder and epilepsy (Sicca et al., 2016, 2011). The reduction of Kir4.1 expression in astrocytes significantly contributes to the etiology of Rett Syndrome (Kahanovitch et al., 2018; Lioy et al., 2011), which shares many pathophysiological traits with SeSAME/EAST. Moreover, Kir4.1 protein is detected as early as embryonic day 20 in glial cells in the developing cortex and hippocampus (Moroni et al., 2015)

suggesting that it could influence neural development in those regions. Thus, mutations in ion channels could affect neurogenesis and have an impact in connectivity resulting in intellectual disabilities. Thus, providing insights into the developmental steps affected by impaired glial-dependent homeostasis we can get closer to understanding the origin of cognitive deficiencies detected in patients with channelopathies or conditions where ion channels in glia are not functional.

MATERIALS AND METHODS

Genetics

Flies were grown in standard medium at 25ºC except for RNAi experiments, which were performed at 29ºC. All genotypes analyzed are specified in the Supplementary Information.

Stocks used to characterize *ClC-a* expression and phenotype were: *MiMIC 05423* (Bloomington Drosophila Stock Center, BDSC 43680), *05423*$^{ClC\text{-}a\text{-}GAL4}$ (BDSC 66801), *MiMIC 14007* (BDSC 59247), *Df(3R)PS2* (BDSC 37742), *mir8-GAL4* (DGRC 104917), *R54H02-GAL4* (BDSC 45784), *wrapper932i-LexA*, *wrapper932i-GAL80* (Coutinho-Budd et al., 2017), *repo-GAL4* on II (Lee and Jones, 2005), *repo-GAL4* on III (BDSC 7415), UAS-Dcr2 (Vienna Drosophila Resource Center, VDRC 60009), *UAS-ClC-a-RNAi* (VDRC 110394), UAS-ClC-a and UAS-rClC2 (this study), *UAS-slit-RNAi* (VDRC 108853), *slit*^{dui} (BDSC 9284), *Slit-GFP* (BDSC 64472), and R9D11-tdtom (BDSC 35847). Additional stocks used in Supplementary Figures were: *ClC-a-GFP* (BDSC 59296), *slit-lacZ* (*Slit*^{05428}) (BDSC 12189), *Rh1GAL4* (BDSC 68385), *Rh4EGFP* (BDSC 7462), *Rh6-lacZ* (BDSC 8117), *GMR-GAL4* (BDSC 1104), *R43H01-LexA* (BDSC 47931) and *R25A01-GAL4* (BDSC 49102), *gcm-lacZ* (BDSC 5445).

To label membranes and nucleus we used *UAS-mCD8-GFP* (BDSC 5137), *UAS-mCD8-RFP.LG* (BDSC 27398), *UAS-mCD8GFP,lexAop-CD2RFP* (BDSC 67093), *UAS-H2B-RFP* (Mayer et al., 2005), *UAS-H2B-YFP* (Bellaïche et al., 2001) as specified in the genotype list. In experiments where nuclear labeling was used for quantification the same transgene was used for control and mutant samples (Fig 5M, Sup Fig 5A).

To generate and label neurogenic tissue clones in the control and *ClC-a* mutant backgrounds (Figure 4D,E and Figure 8J) the following stocks were crossed: *hsFLP,FRT19A,tub-Gal80; tub-GAL4,UAS-mCD8GFP/CyODfYFP; 14007/+* to *FRT19A; +; +* and *hsFLP,FRT19A, tub-Gal80; tub-GAL4,UAS-mCD8GFP/CyODfYFP; 14007/+* to *FRT19A; +; Df(3R)PS2/TM6B.* 3-hour egg lays were kept at 25ºC and clone induction was performed with a 30-minute heat shock pulse at 37ºC in the water bath at the L2 stage. Brains were dissected 48 hours after clone induction.

For lineage tracing experiments (Supplementary Figure 8D-F, G) we used G-TRACE (*UAS-RedStinger,UAS-FLP,Ubi-FRT-stop-FRT-Stinger,* BDSC 28280, (Evans et al., 2009)) combined with specific GAL4 drivers .

When we performed the cortex glia specific rescue experiments (Figure 4J,K and Figure 7B,C) there was no cortex glia specific driver published, so we devised an intersectional genetic strategy to generate one using the *mir8-GAL4* driver. In addition to surface associated cortex glia over the OPC, *mir8-GAL4,* labels cortex glia and neurons in the brain, as well as other cells in the animal. To restrict *mir-8* expression exclusively to cortex glia we combined the following transgenes: *repo-FLP6.2* (Stork et al., 2014), *tub>GAL80>* (BDSC 38879), and *mir8-GAL4*. In this combination GAL4 is only expressed in cortex glia since the GAL80 repressor has only been flipped out in this cell

type but stays in non-glial mir-8 expressing cells (Supplementary Figure 7). For simplicity we refer to this combination as *mir-8* ^{cxg} driver.

DNA constructs

For *UAS-ClC-a* and *UAS-CLCN2* transgenes we used the Gateway cloning System (Invitrogene) and cloned their respective cDNAs into the ΦC31 integrase compatible pBID-UASC-G plasmid (Addgene plasmid # 35202, a gift from Brian McCabe, (Wang et al., 2012)). For the *ClC-a* construct we used the isoform C (a gift from P. Cid) since its electrophysiological properties had already been studied in *Xenopus* oocytes and HEK-293 cells (Flores et al., 2009; Jeworutzki et al., 2012) and this isoform has been described to be expressed in *Drosophila´*s head and body (Flores et al., 2009). The final constructs were injected into the *attp40* (25C6) landing site on the 2nd chromosome.

Immunohistochemistry

Fly brains were dissected in Schneider medium and fixed in 4% PFA in PBL (75mM lysine, 37mM sodium phosphate buffer pH 7,4) for 25 min. After fixation, the tissue was washed in PBS with 0.5%Triton-X-100 (PBST) and blocked with PBST with 10% normal goat serum. Primary and secondary antibody incubations were in PBST and 10% normal goat serum, typically overnight at 4 °C. The following primary antibodies were used for immunohistochemistry: mouse anti-Chaoptin (1:50, 24B10, Developmental Studies Hybridoma Bank, DSHB), rat anti-DE-cadherin (1:50, DCAD2, DSHB), mouse anti-Repo (1:50, 8D12, DSHB), rabbit anti-ClC-a (1:100 this study see Supplementary Information, and 1:100 a gift from J. Dow), guinea pig anti-Deadpan (1:2000, gift from A. Carmena), rat anti-Lethal of scute (1:5000, gift from A. Brand), rabbit anti-Mira (1:500, gift from C. Gonzalez), chicken anti-GFP (1:800, ab13970,

Abcam), rabbit anti-RFP (1:200, 632496, Clonetech), mouse anti-β-galactosidase (1:1000, Z3783, Promega), rabbit anti-β-galactosidase (1:1000, 0855976, Cappl), rabbit anti-Dcp-1 (1:200, Asp216, Cell Signaling). The Alexa Fluor 488, 568 and 647 secondary antibodies raised in rabbit, mouse, rat, guinea pig or chicken (Life technologies) were used at 1:250 concentration. To label the nuclei, TOPRO-3 was used (1:1000, T3605, Life Technologies). Brains were mounted for confocal microscopy in Vectashield (Vector Laboratories). Samples were analyzed with a Leica TCS SPE and a Zeiss LSM880 confocal microscopes.

Photoreceptor phenotype classification

We classified brains as having a strong, medium or weak photoreceptor phenotype based on the OL that out of the two had the more severe phenotype. If not the same, the two OLs tended to be in consecutive categories (i.e. strong/medium, medium/weak, weak/no phenotype). For experiments that entailed photoreceptor phenotypes we always analyzed at least 17 brains.

Measurements and quantifications

To assess adult OL and CB size we took two confocal images of each brain in the appropriate orientations to measure the antero-posterior and dorso-ventral axis of each structure in their widest part. We multiplied those two measurements to obtain a relative value in arbitrary units (a.u). The number of brains analyzed ranged from 23 to 44 for OL (to have fully independent measurements only one OL per brain was quantified) and 12 to 22 for CB when assessing phenotype (Figure 2C, Figure 4H, I). In rescue experiments (Figure 2D, Figure 4J, K), the number of brains analyzed ranged from 12 to 32.

To assess brain size at different larval stages (Figure 4G), the diameter of one larval brain hemisphere per animal was measured in the antero-posterior axis. The *n* ranged from 23 to 37 animals analyzed.

To quantify the number of cortex glia nuclei in late L3 OLs we manually counted ClC-a$^+$ nuclei (Supplementary Figure 5A). Cortex glia nuclei have an average size of approximately 44.5 um2 (Morante et al., 2013) and are clearly distinguishable from ClC-a$^+$ ensheathing glia nuclei by their size and position in the OL. The *n* for this experiment was 8 brains.

To count the number of neuroblasts in the CB part of the hemisphere (Supplementary Figure 5B) we manually identified them based on their nuclear size, and Dpn and Mira antibody staining. Neuroblasts were distinguishable from mature INPs, which are also Dpn$^+$ and Mira$^+$, by a smaller nuclear size and their higher intensity of TOPRO-3 nuclear staining. The *n* for this experiment was 8 brains. To measure neuroepithelia volume the tissue was stained with anti-E-cadherin antibody and manually segmented using the "SURFACE" tool of Imaris software. This tool provides the volume in µm^3 of the generated surfaces (Figure 4B). The *n* for this experiment was between 8 and 9 brains.

To quantify the number of cells in OPC, IPC and CB neuroblast clones (Figure 4D, E) manual counting on confocal stacks was performed. Cells in the clone were identified as TOPRO+ nuclei surrounded by labeled membrane. We counted as many clones as possible per brain as long as they were identifiable as individual clones. The number of clones analyzed in the OPC was of 52 (control) and 31(mutant), in the IPC was 18 (control and mutant), and the number of type I neuroblast clones was 39 (control) and 22 (mutant).

To assess cell death in developing OLs (Figure 4F) we manually counted Dcp-1^{+}/TOPRO $^{+}$ puncta per brain hemisphere. This value was divided by the hemisphere volume obtained through the manual segmentation of the structure and the use of the "SURFACE" tool of Imaris software. The *n* for this experiment was 6 brains.

To quantify the subset of boundary glia among glial cells in the chiasm region at different stages we manually counted ClC-a^{+}/Repo^{+} nuclei (Figure 5M). The *n* for this experiment was 5 brains.

To quantify mature INPs in the DL1 and DL2 lineages (Figure 5U) we manually counted Dpn^{+} positive nuclei surrounded by tdtom^{+} membranes of the *R9D11-tdtomato* marker. To differentiate DL1 from DL2 we used *gcm-lacZ*, which specifically labels the DL2 lineage (Supplementary Figure 9). The *n* for this experiment was between 11 and 12 brains.

To quantify the number of total glial cells in the future chiasm region in mid L3 (Figure 7B) we manually counted Repo^{+} nuclei in confocal stacks. The *n* for this experiment was between 5 and 8 brains.

Image processing

Fiji or Imaris 8.0 (*Bitplane*, South Windsor, CT, USA) were used to process confocal data as specified in figure legends. Figures were assembled using Adobe Illustrator.

Statistics

Statistical analysis was carried out using Prism 6 (GraphPad Software). When data did not follow normality or resulted from a previous mathematical computation (i.e. ratio to volume) we used non-parametric tests. For group comparisons we used Kruskal-Wallis followed by planned pairwise comparisons with Mann-Whitney post hoc test to obtain

p-values (Figure 2C, D; Figure 4B, H, I; Figure 5M; Figure 7B; Supplementary Figure 8H). For pairwise comparisons we used Mann-Whitney's test (Figure 4D, E, F, J, K, Figure 5U, Supplementary Figure 9B). For paired comparisons we used the Wilcoxon matched-pairs squad rank test (Figure 5U)

Data are represented in box plots where the median is represented between the first and third quartiles. Whiskers represent the maximum and minimum values of the data. When all data in the analysis were suitable for a parametric analysis we performed one-way ANOVA followed by Turkey's post hoc test to obtain *p*-values (Figure 4G). *p*-values for pairwise comparisons relevant to our biological inquiry are shown in the bar graph. Data is represented as the mean and error bars show standard deviation.

To evaluate the statistical significance of enhancements in photoreceptor phenotypes qualitatively categorized (i.e. strong, medium, weak, no phenotype) (Figure 6L, M), we performed a Chi-squared test of independence between phenotype categories and genotypes to obtain *p*-values.

ACKNOWLEDGEMENTS

We are grateful to A. Brand, H. Bellen, A. Carmena, P. Cid, J.A. Dow, M. Freeman, C. Gonzalez, B.W. Jones, C. Klambt, J. Morante, I. Salecker, M. Wernet, DSHB, BDSC and VDRC for reagents. We thank V. Hartenstein, J. Modolell, C. González, A. Carmena, J. Tejedor, C. Homem for helpful discussions and suggestions on optic lobe and brain development. We thank F. Aguado, N. Barranco and X. Elorza-Vidal for performing secretion experiments in cell culture. We thank M. Bosch from the Confocal Unit of the CCiT-UB. We thank F. Cebriá for critical reading of the manuscript. Our gratitude to M. Corominas, F. Serras and members of their laboratories for engaging in discussions and making suggestions during our joined lab meetings through out the

project. This work was supported in part by the Spanish Ministerio de Economía y Competitividad grants BFU2015-69689-P to M.M. and M.R, and SAF2015-70377 to R.E.; the Generalitat de Catalunya grant SGR2014-1178 to R.E.; the Institució Catalana de Recerca i Estudis Avançats via an ICREA Academia award to R.E., and an APIF fellowship from the Universitat de Barcelona to H.P-S.

AUTHOR CONTRIBUTIONS

M.M. and R.E conceived the project; M.M., H.P-S., Q.Z., R.E. and H. G-P. designed the experiments and data analysis; H. G-P. and R.E. contributed reagents and analytical tools; M. R. designed the statistical analysis; H.P-S. and Q.Z. performed the experiments; H.P-S., Q.Z, M.R. and M.M. analyzed results; and M.M. wrote the manuscript with contributions from all the other authors.

FIGURE LEGENDS

Figure 1. *ClC-a* is expressed in cortex glia and ensheathing glia during brain development.

(A-I) Analysis of *ClC-a* expression in the developing brain. Brain illustrations show the orientation of imaging planes for the indicated panels at different larval stages. *ClC-a* specific GAL4 driver (*ClC-a-GAL4)* was used to label cellular membranes (green) and nucleus (red) of ClC-a^{+} cells. Glial nuclei were labeled with anti-Repo antibody (blue). Anti-E-cadherin (E-cad, magenta) was used to identify neuroepithelial cells. Neuroblasts and photoreceptors were labeled with anti-Deadpan (Dpn, grey) and anti-Chaoptin (24B10, grey) respectively. (A-B) Lateral view of L1 brain hemispheres outlined with a dashed line. A' shows Repo staining from A. (C, D) Horizontal views of L2 brain hemispheres. (E, F) Horizontal views at the surface of late L3 brain

hemispheres. Asterisks in E mark examples of cortex glia chambers. (G) Horizontal view through the middle of the L3 brain hemisphere. The lamina furrow (LF) is the indentation where OPC gives rise to LPCs in the lateral side. (H) Horizontal view at the same level as G, showing the region demarcated by the dashed box in the schematic on the right. Photoreceptors enter the brain through the LPC region. (I) Frontal view of a volume rendering 3D reconstruction of the OL corresponding to the region demarcated by the dashed square in the schematic on top. The membranes of ClC-a$^+$ glial nuclei created a barrier that separated the developing lamina and LoP. (J-Q) Identification of ClC-a$^+$ glial types. (J-K) Characterization of ClC-a$^+$ cells over the OPC. (J) Analysis of ClC-a$^+$ nuclear position with respect to the BBB. (K) Colocalization analysis of ClC-a protein with *mir-8*. Expression in LF is marked by an arrow and expression between the LPC and the LoP is marked by arrowheads. (L-N) Confirmation of *ClC-a* expression in cortex glia. (L) Membrane and nuclear patterns obtained with the *wrapper* GAL4 driver (*R54H02-GAL4)* For similarity to *ClC-a-GAL4* generated patterns compare to panel G. (M-N) Colocalization study of membrane patterns generated by the *ClC-a-GAL4* driver and a *LexA* driver version of the cortex glia *wrapper* driver (*wrapper932i-LexA*) using *UAS* and *lexAop* fluorescent reporters. (M) Horizontal view on the surface of the brain. To visualize *ClC-a* expression (green) in the CB (dashed region of interest) gain had to be elevated with the consequent saturation of the expression in the OL. M' and M" show *ClC-a* (green) and *wrapper* expression (red) respectively from region of interest in M. (N) Deeper section into the hemisphere imaged with gain conditions to analyze OL colocalization, thus *ClC-a* signal (green) in the CB is very low. N' and N" show *ClC-a* (green) and *wrapper* (red) membrane signals. (O-Q) Identification of non-cortex glia ClC-a$^+$ cells as ensheathing glia. (O) *ClC-a* is expressed in neuropil-ensheathing glia (eng) surrounding CB neuropils, and tract-ensheathing glia wrapping the mushroom

body peduncle (Pe, inset). (P) *ClC-a* is expressed in glia surrounding the mushroom body calyx. (Q) ClC-a is expressed in palisade glia and in the outer chiasm glia (Xg_o), which wrapps photoreceptor axons in their transition from the lamina to the medulla neuropils.

OPC, outer proliferation center; IPC, inner proliferation center; OL, optic lobe; CB, central brain; LF, lamina furrow; LPC, lamina precursor cells; LoP, lobula plug; cxg, cortex glia; sg, satellite glia; pag, palisade glia; eg, epithelial glia; mg, marginal glia; Xg_o, outer chiasm glia; BBB, blood brain barrier; Pe, peduncle; egn, ensheathing glia of neuropil; Ca, calyx. Scale bars represent 10 µm.

(See also Supplementary Figures 1 and 2)

Figure 2. *ClC-a* mutants have smaller brains and photoreceptor guidance defects.

(A) Schematic of the *ClC-a* transcripts in the *ClC-a* locus and the insertion location of *Mi(MIC)ClC-a*^{05423} and *Mi(MIC)ClC-a*^{14007} transposons. (B) Magnification of the pink dashed box around *Mi(MIC)ClC-a*^{05423} in A. The original *Mi(MIC)* transposon cassette contains a splice acceptor followed by stop codons in all reading frames is followed by the EGFP coding sequence with a polyadenylation signal. When inserted in an intron between coding exons in the orientation of gene transcription, the use of the transposon's splice acceptor generates truncated transcripts. The Trojan-GAL4 cassette swapped by RMCE to generate *05423*$^{ClC\text{-}a\text{-}GAL4}$ contains a splice acceptor that ensures that the T2A-GAL4 open reading frame is included in the mRNA of the *ClC-a* gene. The T2A sequence promotes the separate translation of GAL4. (C-D) Quantification of OL size in arbitrary units. *p*-values were calculated with the non-parametric Mann-Whitney test. (C) Comparison of OL size of two *ClC-a* mutant allelic combinations, *05423*$^{ClC\text{-}a\text{-}GAL4}$*/14007* and *05423*$^{ClC\text{-}a\text{-}GAL4}$*/Df*, to their respective controls. (D)

Comparison of OL size of *05423*$^{ClC\text{-}a\text{-}GAL4}$*/Df* to mutant brains in which *ClC-a (UAS-ClC-a)* or rat *CLCN2* (*UAS-CLCN2*) mRNAs were expressed in glia. (E-I) Characterization of photoreceptor guidance defects. (E) Confocal section of an adult OL of an heterozygous control animal (*14007/+)* showing the wild type photoreceptor array stained with anti-Chaoptin (24B10, green). The schematic shows the trajectory of R7 and R8 photoreceptor axons. (F) Confocal images of adult OLs of the *14007/Df* mutant allelic combination classified according to phenotype severity (no phenotype, weak, mild and strong). For simplicity, the schematic depicts the altered trajectory of the R7 and R8 axons of a single ommatidium. To show the complete trajectory of misguided photoreceptors, images for the weak and medium phenotypes are Z-projections of confocal stacks. (G-I) Photoreceptor phenotype analysis for different experiments. Phenotype penetrance and expressivity for each condition is depicted as the percentage of brains with no phenotype, weak, medium and strong phenotypes (see Material and Methods). Heterozygous controls in (G) and (H) shown no phenotype. (G) Classification of *ClC-a* mutant allelic combinations according to their penetrance and expressivity strength. (H) Analysis of glia specific knock down of *ClC-a* using RNAi. (I) Glia specific rescue experiment using *ClC-a* and rat *CLCN2* mRNAs in two allelic combinations *14007/Df* and *05423*$^{ClC\text{-}a\text{-}GAL4}$*/Df*.

Scale bars represent 10 µm. ** $p<0.01$, *** $p<0.001$.

(See also Supplementary Figures 3 and 4)

Figure 3. The cortex glia membrane scaffold remains unaltered in *ClC-a* mutant animals.

Analysis of cortex glia membrane scaffold (green) and nuclear (red) distribution in control (*05423*$^{ClC\text{-}a\text{-}GAL4}$/+) and mutant (*05423*$^{ClC\text{-}a\text{-}GAL4}$*/14007*) brain hemispheres.

Horizontal views at specified developmental times and depths are shown. (A, B) View through the middle of the early (A) and late (B) L3 hemisphere of a control animal. Anti-E-cadherin (E-cad, magenta) labels neuroepithelial cells. (C) View of the surface of a control brain stained with anti-Deadpan (Dpn, grey) to visualize neuroblasts. (D, D') Slightly deeper view of the surface of a control brain stained with anti-Elav to visualize postmitotic neurons. (E), (F), (G) and (H, H') panels are equivalent views and stainings in mutant animals.

OPC, outer proliferation center; IPC, inner proliferation center. Scale bars represent 10 µm.

(See also Supplementary Figure 5)

Figure 4. *ClC-a* is required for the proliferation of neurepithelial cells and neuroblasts, as well as neuronal viability and sufficient to rescue brain size.

p-values of indicated comparisons were calculated with the non-parametric Mann-Whitney test unless otherwise stated. (A) Images of surface rendering 3D reconstructions of the OPC (magenta) and IPC (cyan) shown from the lateral and posterior views, in control (*14007/+*) and mutant (*14007/Df)* brains. Bracket indicates the absence of the central domain of the OPC in mutant late L3 reconstructions. (B) Quantification and comparison of the volume in μm^3 of reconstructed OPC (magenta) and IPC (cyan) of mid and late control and mutant animals. (C) Analysis of cell death in mid L3 OPC and IPC (E-cad, grey) of control and mutant animals using anti-Dcp-1 staining (Dcp-1, green) to label apoptotic cells. Nuclei (red) are labeled with TOPRO-3. Confocal sections show that apoptotic cells in control and mutant tissue were found outside the neuroepithelial cells. (D) Images of volume rendering 3D reconstructions of control and mutant mid L3 OLs that happen to have mitotic clones (green) both in the

OPC and IPC. Anti-E-cadherin (E-cad, grey) labels neuroepithelial cells. Magenta and blue spheres represent cells in OPC and IPC clones respectively. Quantification and comparison of the number of cells per OPC and IPC clones in the control and mutant background is shown. (E) Images of volume rendering 3D reconstructions of segmented mitotic clones in type I neuroblast in mid L3 control and mutant animals. The clone is labeled in green. Anti-Dpn staining (Dpn, red) identifies the neuroblast. TOPRO-3 labels the nuclei of cells in the clone. Quantification of the number of cells per clone in type I neuroblast clones in control and mutant animals and their comparison is shown. (F) Quantification and comparison of cell death (Dcp-1^{+}/TOPRO-3^{+} puncta) in mid L3 brain hemispheres. (G) Graphic showing the diameter of larval hemispheres at different L3 stages in control and mutant animals. Error bars indicate Standard Deviation. Comparisons between control and mutant diameters at each larval stage are shown. *p*-values were calculated with the parametric Turkey's test. The growth rate between larval stages in controls and mutants is indicated at the top of the graphic. (H, I) Quantifications and comparisons of adult OL (H) and CB (I) size for *14007/Df* animals and controls. (J, K) Quantifications and comparisons of adult OL (J) and CB (K) size in cortex glia specific rescue experiment brains and the appropriate controls. Control brains represent genotypes for both the GAL4 driver and the UAS transgene in the mutant background since they could not be distinguished in the genetic scheme of the experiment (*mir-8*^{glia} control and *UAS-ClC-a* control). For cortex glia specific driver details refer to Materials and Methods and Supplementary Figure 7.

OPC, outer proliferation center; IPC, inner proliferation center. Scale bars represent 10 µm. n.s.>0.05, ** p<0.01, *** p<0.001.

(See also Supplementary Figures 6 and 7)

Figure 5. Strong reduction of a subset of ClC-a$^+$ ensheathing glial cells and defects in the neuroblast that originates them are observed in *ClC-a* mutants.

(A-M) Developmental analysis of cells that express *ClC-a* in the OL region in control animals (*05423*$^{ClC\text{-}a\text{-}GAL4}$ /+) and those same cells in *ClC-a* mutant animals (*05423*$^{ClC\text{-}a\text{-}GAL4}$ */14007*). Cortex glia membranes are shown in green and nuclei in red. All glial nuclei were labeled with anti-Repo antibody (blue). (A-D) Images of the ClC-a$^+$ glial barrier from early to late L3 control OLs with the corresponding schematics, in frontal views (A-C) and horizontal view (D). (A-C) are volume rendering 3D reconstructions to show ClC-a$^+$ boundary glia population in early (A) and in mid (B) L3, and its split into pag and Xg_o in late L3 (C). (D) is a confocal section. The schematic includes photoreceptors, not labeled in (D) but shown in (F). (E) *ClC-a* expression pattern in the adult OL. The inner and outer chiasms are correctly formed. (F) Photoreceptor axons (24B10, grey) in late L3 OLs. For their relative position to glia refer to the horizontal view schematic. (G-J) Images showing which of the glial cells that would normally express *ClC-a* in control OLs are still present in *ClC-a* mutant OLs from early to late L3 larval stages with the corresponding schematics, in frontal views (G-I) and horizontal view (J). (G-I) are volume rendering 3D reconstructions. (J) is a confocal section. The schematic shows the aberrant trajectory that some photoreceptor axons can take in (L). (K) *ClC-a* expression pattern in the mutant adult OL. The inner and outer chiasms are defective. (L) Photoreceptor axons (24B10, grey) in late L3 mutant OLs. For their relative position to glia refer to the horizontal view schematic. (M) Quantification and comparison of ClC-a$^+$/Repo$^+$ nuclei in the OL region. *p*-values were calculated with the non-parametric Mann-Whitney test. (N-U) Analysis of type II DL neuroblast lineages in the CB. (N) Schematic showing the relative position of DM and DL lineages. (O-Q) Volume rendering 3D reconstructions of late L3 control (*14007/+*, O) and mutant

(*14007/Df*, P, Q) brain hemispheres showing type II lineages labeled with the R9D11-tdtomato (red). Grey and blue spheres mark the position of the DM and DL neuroblasts respectively. (R) Confocal image showing the DL1/2 cluster lineages (red), the neuroblast (asterisk) and mature INPs (arrowheads) labeled with anti-Deadpan (Dpn, blue) and cortex glia membranes (green) surrounding the neuroblast and encasing the lineage in a glial chamber. (S, T) Volume rendering 3D reconstructions of a DL1/2 cluster lineages (red) of a control (S) and mutant (T) brains where blue spheres mark the neuroblasts and smaller yellow spheres mark mature INPs of one of the lineages and green spheres from the other lineage. (U) Quantification of the number of INPs per DL lineage. Comparisons between the INP number in the two lineages (green and yellow box plots) of controls and of mutants are shown. *p*-values were calculated by the non parametric Wilcoxon matched-pairs squad rank test. Comparison of number of INPs of lineages with the highest INPs (green box plots) between control and mutants is shown. Comparison of number of INPs of lineages with the lowest INPs (yellow box plots) between control and mutants is shown. In both comparisons *p*-values were calculated with the non-parametric Mann-Whitney test.

OPC, outer proliferation center; IPC, inner proliferation center; cxg, cortex glia; bg, boundary glia; sg, satellite glia; pag, palisade glia; Xg_o, outer chiasm glia; eg, epithelial glia; mg, marginal glia; me, medulla. Scale bars represent 10 µm. * $p<0.05$ ** $p<0.01$, *** $p<0.001$.

(See also Supplementary Figures 8 and 9)

Figure 6. Boundary glia, which expresses the chemorepellent molecule Slit, is in close contact with photoreceptor axons as they innervate the OL.

(A-D) Spatiotemporal relationship between photoreceptors and boundary glia cells. Number of photoreceptor rows was inferred from 24B10^{+} rows in the eye imaginal disc. (A, B) Horizontal views of mid L3 optic lobe showing ClC-a^{+} glia and one (A) and two (B) rows of R8 photoreceptors (Chaoptin, grey). (C) Same view and staining as panels A and B of a slightly older brain innervated by six rows of photoreceptors. (D) Frontal view showing, between the line of Xg$_{o}$ cell bodies tranversal sections of photoreceptors on their way to the medulla. (E, F) Larval (E) and adult (F) examples of photoreceptor (24B10, grey) phenotypes in *ClC-a* mutants classified as strong. (G, H) Larval (G) and adult (H) photoreceptor (GMR-GFP, grey) phenotypes in *slit^{dui}* mutants. Arrowheads show misguided axons innervating the medulla from its proximal face. (I-K) Developmental analysis of Slit expression in glial cells in the barrier. Schematics for the view in each of the stages analyzed are shown. (J) and (K) schematics include photoreceptors for orientation although they are not labeled in the images. Anti-Repo (blue) was used to label glial nuclei. A Slit-GFP protein trap (*sli[MI03825-GFSTF.2]*) that outlines membranes of *slit* expressing cells (Supplementary Figure 10) was used to visualize *slit* the expression pattern (red, I'-K'). ClC-a^{+} boundary glia (green, I"-K") are outlined (white dashed line) in (I-I",J-J"). Xg$_{o}$ and palisade glia are outlined in (K-K"). Although in (K") their *ClC-a* expression is downregulated, we have shown that they express *ClC-a* in other panels (Fig 1H, Fig 5D, 5P, Supplementary Figure 6K). (I) Frontal view of an early L3 OL. (J) Horizontal view of a mid L3 OL. (K) Horizontal view of a late L3 OL. (L, M) Phenotype analysis for *slit/ClC-a* genetic interaction (M) and *slit* knockdown (L). Phenotype penetrance and expressivity for each condition is depicted as the percentage of brains with no phenotype, weak, medium and strong phenotypes. n ≥ 20 brains for condition. *p*-values were calculated with the Chi square test.

cxg, cortex glia; bg, boundary glia; Bn, Bolwigs nerve; Lp, lamina plexus; Xg_o, outer chiasm glia; sg, satellite glia; OPC, outer proliferation center; IPC, inner proliferation center; eg, epithelial glia; mg, marginal glia; pag, palisade glia; me, medulla. Scale bars represent 10 µm. * $p<0.05$.

(See also Supplementary Figure 10).

Figure 7. *ClC-a* expression exclusively in cortex glia rescues the formation of boundary glia and the photoreceptor guidance defects.

(A) Schematics depicting the cortex glia specific rescue experiment. Frontal views of mid L3 OLs and the DL1 lineage: control (*14007/+*) showing glial nuclei in blue (Repo) and *ClC-a* expression in green in the CB in cortex glia surrounding the DL1 neuroblast and its progeny, and in the OL in cortex glia over the neuroepitheliums and boundary glia; a *ClC-a* mutant (*14007/Df*) showing the absence of *ClC-a* expression and boundary glia; and an animal where *ClC-a* expression is exclusively restored in cortex glia ($mir\text{-}8^{cxg}$) results in the recovery of boundary cortex glia that does not express ClC-a because it is a subtype of ensheathing glia. (B) Quantification and comparisons of glial nuclei (Repo, blue) in control, mutant and rescue animals. *p*-values were calculated with the non-parametric Mann-Whitney test. (C) Quantification of photoreceptor guidance phenotypes in control and rescue brains. Control brains represent genotypes for both the GAL4 driver and the UAS transgene since they could not be distinguished in the genetic scheme of the experiment. ($mir\text{-}8^{glia}$ control and *UAS-ClC-a* control).

Scale bars represent 10 µm. * $p<0.05$, ** $p<0.01$, *** $p<0.001$.

Figure 8. Guidance defects in mushroom body neurons.

(A) Schematic of a mushroom body in one hemisphere. Dashed lines indicate the position of imaging planes and associated letters indicates correspondence to panels. The axonal component of the mushroom body, the peduncle and lobes, are shown in red representing anti-Fasciclin II (FasII) antibody staining. (B-E) Mushroom body analysis in control brains (late L3 *05423*$^{ClC\text{-}a\text{-}GAL4}$ /+ or mid L3 *14007*/+). (B) Confocal section though the calyx region of a control brain showing ClC-a^{+} glial membranes (green) and all nuclei (blue, TOPRO-3). (C) Transversal section through the peduncle of a control brain (D) Longitudinal section of the peduncle showing ClC-a^{+} tract ensheating glia surrounding it (arrow). (E) Volume rendering 3D reconstruction of a control brain hemisphere showing N-cadherin positive neuropils . (F-I) Mushroom body analysis in *ClC-a* mutant brains (late L3 *05423*$^{ClC\text{-}a\text{-}GAL4}$ */14007* or mid L3 *14007/Df*) with the same staining as the equivalent control panels. Compare to panel (F) to (B), (G) to (C), (H) to (D), (I) to (E). (J-O) Schematic (J) and volume rendering 3D reconstructions and confocal sections of mushroom body neuroblast clones in control (K, L) and *ClC-a* mutant (M-O) brains labeled in green. (K) Control clone. (L) Cross section of a control clone at the level of the peduncle. (M) Mutant clone. (N) Cross section at the level of the peduncle of a mutant clone in M. (O) Mutant clone with a strong phenotype.

Ca, calyx; Pe, peduncle; mL, medial lobe; vL, vertical lobe. Scale bars represent 10 µm.

REFERENCES

Apitz H, Salecker I. 2015. A region-specific neurogenesis mode requires migratory progenitors in the Drosophila visual system. *Nat Neurosci* **18**. doi:10.1038/nn.3896

Apitz H, Salecker I. 2014. A challenge of numbers and diversity: Neurogenesis in the drosophila optic lobe. *J Neurogenet* **28**:233–249. doi:10.3109/01677063.2014.922558

Bailey AP, Koster G, Guillermier C, Hirst EMA, MacRae JI, Lechene CP, Postle AD, Gould AP. 2015. Antioxidant Role for Lipid Droplets in a Stem Cell Niche of Drosophila. *Cell* **163**:340–353. doi:10.1016/j.cell.2015.09.020

Barres BA. 1991. Glial ion channels. *Curr-Opin-Neurobiol* **1**:354–4388. doi:10.1016/0959-4388(91)90052-9

Barres B a, Chun LL, Corey DP. 1990. Ion channels in vertebrate glia. *Annu Rev Neurosci* **13**:441–474. doi:10.1146/annurev.neuro.13.1.441

Bazargani N, Attwell D. 2016. Astrocyte calcium signaling: the third wave. *Nat Neurosci* **19**:182.

Bellaïche Y, Gho M, Kaltschmidt JA, Brand AH, Schweisguth F. 2001. Frizzled regulates localization of cell-fate determinants and mitotic spindle rotation during asymmetric cell division. *Nat Cell Biol* **3**:50–57. doi:10.1038/35050558

Bellot-Saez A, Kékesi O, Morley JW, Buskila Y. 2017. Astrocytic modulation of neuronal excitability through K+spatial buffering. *Neurosci Biobehav Rev* **77**:87–97. doi:10.1016/j.neubiorev.2017.03.002

Bjornsson CS, Apostolopoulou M, Tian Y, Temple S. 2015. It takes a village: Constructing the neurogenic niche. *Dev Cell* **32**:435–446. doi:10.1016/j.devcel.2015.01.010

Black JA, Waxman SG. 2013. Noncanonical roles of voltage-gated sodium channels. *Neuron* **80**:280–291. doi:10.1016/j.neuron.2013.09.012

Blanz J, Schweizer M, Auberson M, Maier H, Muenscher A, Hübner C a, Jentsch TJ. 2007. Leukoencephalopathy upon disruption of the chloride channel ClC-2. *J Neurosci* **27**:6581–9. doi:10.1523/JNEUROSCI.0338-07.2007

Bockenhauer D, Tobin J, Ph D, Lieberer E, Sterner C, Sc M, Hoff W Van, Masri O Al, Tullus K, Ph D, Arcos-burgos M, Ph D, Knepper MA, Ph D. 2009. Epilepsy,

Ataxia, Sensorineural Deafness, Tubulopathy, and.

Boone JQ, Doe CQ. 2008. Identification of Drosophila type II neuroblast lineages containing transit amplifying ganglion mother cells. *Dev Neurobiol* **68**:1185–1195. doi:10.1002/dneu.20648

Bösl MR, Stein V, Hübner C, Zdebik a a, Jordt SE, Mukhopadhyay a K, Davidoff MS, Holstein a F, Jentsch TJ. 2001. Male germ cells and photoreceptors, both dependent on close cell-cell interactions, degenerate upon ClC-2 Cl(-) channel disruption. *EMBO J* **20**:1289–99. doi:10.1093/emboj/20.6.1289

Cabrero P, Terhzaz S, Romero MF, Davies SA, Blumenthal EM, Dow JAT. 2014. Chloride channels in stellate cells are essential for uniquely high secretion rates in neuropeptide-stimulated *Drosophila* diuresis. *Proc Natl Acad Sci* **111**:14301–14306. doi:10.1073/pnas.1412706111

Carswell KS, Papoutsakis ET. 2000. Extracellular pH affects the proliferation of cultured human T cells and their expression of the interleukin-2 receptor. *J Immunother* **23**:669–674. doi:10.1097/00002371-200011000-00008

Catalán M, Niemeyer MI, Cid LP, Sepúlveda F V. 2004. Basolateral ClC-2 Chloride Channels in Surface Colon Epithelium: Regulation by a Direct Effect of Intracellular Chloride. *Gastroenterology* **126**:1104–1114. doi:10.1053/j.gastro.2004.01.010

Celniker SE, Dillon LAL, Gerstein MB, Gunsalus KC, Henikoff S, Karpen GH, Kellis M, Lai EC, Lieb JD, MacAlpine DM, Micklem G, Piano F, Snyder M, Stein L, White KP, Waterston RH. 2009. Unlocking the secrets of the genome. *Nature* **459**:927–930. doi:10.1038/459927a

Chell JM, Brand AH. 2010. Nutrition-responsive glia control exit of neural stem cells from quiescence. *Cell* **143**:1161–1173. doi:10.1016/j.cell.2010.12.007

Chen C, Ouyang W, Grigura V, Zhou Q, Carnes K, Lim H, Zhao GQ, Arber S, Kurpios N, Murphy TL, Cheng AM, Hassell JA, Chandrashekar V, Hofmann MC, Hess RA, Murphy KM. 2005. ERM is required for transcriptional control of the spermatogonial stem cell niche. *Nature* **436**:1030–1034. doi:10.1038/nature03894

Cheng LY, Bailey AP, Leevers SJ, Ragan TJ, Driscoll PC, Gould AP. 2011. Anaplastic lymphoma kinase spares organ growth during nutrient restriction in drosophila. *Cell* **146**:435–447. doi:10.1016/j.cell.2011.06.040

Chotard C, Salecker I. 2008. Glial cell development and function in the Drosophila visual system. *Neuron Glia Biol* **3**:17–25. doi:10.1017/S1740925X07000592.Glial

Chotard C, Salecker I. 2004. Neurons and glia: Team players in axon guidance. *Trends Neurosci* **27**:655–661. doi:10.1016/j.tins.2004.09.001

Ciapa B, Philippe L. 2013. Intracellular and Extracellular pH and Ca Are Bound to Control Mitosis in the Early Sea Urchin Embryo via ERK and MPF Activities. *PLoS One* **8**. doi:10.1371/journal.pone.0066113

Corty MM, Freeman MR. 2013. Architects in neural circuit design: Glia control neuron numbers and connectivity. *J Cell Biol* **203**:395–405. doi:10.1083/jcb.201306099

Coutinho-Budd JC, Sheehan AE, Freeman MR. 2017. The secreted neurotrophin spätzle 3 promotes glial morphogenesis and supports neuronal survival and function. *Genes Dev* **31**:2023–2038. doi:10.1101/gad.305888.117

Dearborn R. 2004. An axon scaffold induced by retinal axons directs glia to destinations in the Drosophila optic lobe. *Development* **131**:2291–2303. doi:10.1242/dev.01111

Denholm B, Hu N, Fauquier T, Caubit X, Fasano L, Skaer H. 2013. The tiptop/teashirt genes regulate cell differentiation and renal physiology in Drosophila. *Development* **140**:1100–1110. doi:10.1242/dev.088989

Depienne C, Bugiani M, Dupuits C, Galanaud D, Touitou V, Postma N, van Berkel C,

Polder E, Tollard E, Darios F, Brice A, de Die-Smulders CE, Vles JS, Vanderver A, Uziel G, Yalcinkaya C, Frints SG, Kalscheuer VM, Klooster J, Kamermans M, Abbink TEM, Wolf NI, Sedel F, van der Knaap MS. 2013. Brain white matter oedema due to ClC-2 chloride channel deficiency: An observational analytical study. *Lancet Neurol* **12**:659–668. doi:10.1016/S1474-4422(13)70053-X

Diao F, Ironfield H, Luan H, Diao F, Shropshire WC, Ewer J, Marr E, Potter CJ, Landgraf M, White BH. 2015. Plug-and-play genetic access to drosophila cell types using exchangeable exon cassettes. *Cell Rep* **10**:1410–1421. doi:10.1016/j.celrep.2015.01.059

Doe CQ. 2008. Neural stem cells: balancing self-renewal with differentiation. *Development* **135**:1575–1587. doi:10.1242/dev.014977

Dumstrei K, Wang F, Hartenstein V. 2003. Role of DE-cadherin in neuroblast proliferation, neural morphogenesis, and axon tract formation in *Drosophila* larval brain development. *J Neurosci* **23**:3325–3335.

Edwards MM, Marín de Evsikova C, Collin GB, Gifford E, Wu J, Hicks WL, Whiting C, Varvel NH, Maphis N, Lamb BT, Naggert JK, Nishina PM, Peachey NS. 2010. Photoreceptor degeneration, azoospermia, leukoencephalopathy, and abnormal RPE cell function in mice expressing an early stop mutation in CLCN2. *Invest Ophthalmol Vis Sci* **51**:3264–72. doi:10.1167/iovs.09-4887

Egger B, Gold KS, Brand AH. 2010. Notch regulates the switch from symmetric to asymmetric neural stem cell division in the Drosophila optic lobe. *Development* **137**:2981–2987. doi:10.1242/dev.051250

Evans CJ, Olson JM, Ngo KT, Kim E, Lee NE, Kuoy E, Patananan AN, Sitz D, Tran PT, Do MT, Yackle K, Cespedes A, Hartenstein V, Call GB, Banerjee U. 2009. G-TRACE: Rapid Gal4-based cell lineage analysis in Drosophila. *Nat Methods*

6:603–605. doi:10.1038/nmeth.1356

Fan Y, Soller M, Flister S, Hollmann M, Müller M, Bello B, Egger B, White K, Schäfer MA, Reichert H. 2005. The egghead gene is required for compartmentalization in Drosophila optic lobe development. *Dev Biol* **287**:61–73. doi:10.1016/j.ydbio.2005.08.031

Fietz SA, Kelava I, Vogt J, Wilsch-Bräuninger M, Stenzel D, Fish JL, Corbeil D, Riehn A, Distler W, Nitsch R, Huttner WB. 2010. OSVZ progenitors of human and ferret neocortex are epithelial-like and expand by integrin signaling. *Nat Neurosci* **13**:690–699. doi:10.1038/nn.2553

Flinck M, Kramer SH, Pedersen SF. 2018. Roles of pH in control of cell proliferation. *Acta Physiol* **223**:1–17. doi:10.1111/apha.13068

Flores CA, Niemeyer MI, Sepúlveda F V, Cid LP. 2009. Two splice variants derived from a Drosophila melanogaster candidate ClC gene generate ClC-2-type Cl-channels. *Mol Membr Biol* **23**:149–56. doi:10.1080/09687860500449978

Földy C, Lee SH, Morgan RJ, Soltesz I. 2010. Regulation of fast-spiking basket cell synapses by the chloride channel ClC-2. *Nat Neurosci* **13**:1047–1049. doi:10.1038/nn.2609

Freeman MR, Doherty J. 2006. Glial cell biology in Drosophila and vertebrates. *Trends Neurosci* **29**:82–90. doi:10.1016/j.tins.2005.12.002

González F, Romani S, Cubas P, Modolell J, Campuzano S. 1989. Molecular analysis of the asense gene, a member of the achaete-scute complex of Drosophila melanogaster, and its novel role in optic lobe development. *EMBO J* **8**:3553–3562. doi:10.1002/J.1460-2075.1989.TB08527.X

Han C, Jan LY, Jan Y-N. 2011. Enhancer-driven membrane markers for analysis of nonautonomous mechanisms reveal neuron-glia interactions in Drosophila. *Proc*

Natl Acad Sci **108**:9673–9678. doi:10.1073/pnas.1106386108

Hansen D V., Lui JH, Parker PRL, Kriegstein AR. 2010. Neurogenic radial glia in the outer subventricular zone of human neocortex. *Nature* **464**:554–561. doi:10.1038/nature08845

Hoegg-Beiler MB, Sirisi S, Orozco IJ, Ferrer I, Hohensee S, Auberson M, Gödde K, Vilches C, De Heredia ML, Nunes V, Estévez R, Jentsch TJ. 2014. Disrupting MLC1 and GlialCAM and ClC-2 interactions in leukodystrophy entails glial chloride channel dysfunction. *Nat Commun* **5**. doi:10.1038/ncomms4475

Hofbauer A, Campos-Ortega J. 1990. Proliferation and and early differentiation of the optic lobes in Drosophila melanogaster. *Roux's Arch Dev Biol* 264–274.

Hou X, Zhang R, Wang J, Li Y, Li F, Zhang Y, Zheng X, Shen Y, Wang Y, Zhou L. 2018. CLC-2 is a positive modulator of oligodendrocyte precursor cell differentiation and myelination. *Mol Med Rep* **17**:4515–4523. doi:10.3892/mmr.2018.8439

Hoyle G, Williams M, Phillips C. 1986. Functional morphology of insect neuronal cell surface/glial contacts: The trophospongium. *J Comp Neurol* **256**:113–28.

Jentsch TJ, Pusch M. 2018. CLC Chloride Channels and Transporters: Structure, Function, Physiology, and Disease. *Physiol Rev* **98**:1493–1590. doi:10.1152/physrev.00047.2017

Jeworutzki E, López-Hernández T, Capdevila-Nortes X, Sirisi S, Bengtsson L, Montolio M, Zifarelli G, Arnedo T, Müller CS, Schulte U, Nunes V, Martínez A, Jentsch TJ, Gasull X, Pusch M, Estévez R. 2012. GlialCAM, a protein defective in a leukodystrophy, serves as a ClC-2 Cl(-) channel auxiliary subunit. *Neuron* **73**:951–61. doi:10.1016/j.neuron.2011.12.039

Jordt SE, Jentsch TJ. 1997. Molecular dissection of gating in the CIC-2 chloride

channel. *EMBO J* **16**:1582–1592. doi:10.1093/emboj/16.7.1582

Kahanovitch U, Cuddapah VA, Pacheco NL, Holt LM, Mulkey DK, Percy AK, Olsen ML. 2018. MeCP2 Deficiency Leads to Loss of Glial Kir4.1. *Eneuro* **2**:ENEURO.0194-17.2018. doi:10.3923/JBS.2017.394.399

Kanai MI, Kim MJ, Akiyama T, Takemura M, Wharton K, O'Connor MB, Nakato H. 2018. Regulation of neuroblast proliferation by surface glia in the Drosophila larval brain. *Sci Rep* **8**:1–15. doi:10.1038/s41598-018-22028-y

Karres JS, Hilgers V, Carrera I, Treisman J, Cohen SM. 2007. The Conserved microRNA MiR-8 Tunes Atrophin Levels to Prevent Neurodegeneration in Drosophila. *Cell* **131**:136–145. doi:10.1016/j.cell.2007.09.020

Kearney JB, Wheeler SR, Estes P, Parente B, Crews ST. 2004. Gene expression profiling of the developing Drosophila CNS midline cells. *Dev Biol* **275**:473–492. doi:10.1016/j.ydbio.2004.08.047

Khakh BS, McCarthy KD. 2015. Astrocyte calcium signaling: From observations to functions and the challenges therein. *Cold Spring Harb Perspect Biol* **7**:1–18. doi:10.1101/cshperspect.a020404

Kremer MC, Jung C, Batelli S, Rubin GM, Gaul U. 2017. The glia of the adult Drosophila nervous system. *Glia* **65**:606–638. doi:10.1002/glia.23115

Lee BP, Jones BW. 2005. Transcriptional regulation of the Drosophila glial gene repo. *Mech Dev* **122**:849–862. doi:10.1016/j.mod.2005.01.002

Li G-R. 2011. Functional ion channels in stem cells. *World J Stem Cells* **3**:19. doi:10.4252/wjsc.v3.i3.19

Liebau S, Kleger A, Levin M, Yu SP. 2013. Stem cells and ion channels. *Stem Cells Int* **2013**. doi:10.1155/2013/238635

Lioy DT, Garg SK, Monaghan CE, Raber J, Foust KD, Kaspar BK, Hirrlinger PG,

Kirchhoff F, Bissonnette JM, Ballas N, Mandel G. 2011. A role for glia in the progression of Rett-syndrome. *Nature* **475**:497–500. doi:10.1038/nature10214

Makara JK, Rappert A, Matthias K, Steinhäuser C, Spät A, Kettenmann H. 2003. Astrocytes from mouse brain slices express ClC-2-mediated Cl-currents regulated during development and after injury. *Mol Cell Neurosci* **23**:521–530. doi:10.1016/S1044-7431(03)00080-0

Mayer B, Emery G, Berdnik D, Wirtz-Peitz F, Knoblich JA. 2005. Quantitative analysis of protein dynamics during asymmetric cell division. *Curr Biol* **15**:1847–1854. doi:10.1016/j.cub.2005.08.067

Morante J, Vallejo DM, Desplan C, Dominguez M. 2013. Conserved miR-8/miR-200 defines a glial niche that controls neuroepithelial expansion and neuroblast transition. *Dev Cell* **27**:174–187. doi:10.1016/j.devcel.2013.09.018

Moroni RF, Inverardi F, Regondi MC, Pennacchio P, Frassoni C. 2015. Developmental expression of Kir4.1 in astrocytes and oligodendrocytes of rat somatosensory cortex and hippocampus. *Int J Dev Neurosci* **47**:198–205. doi:10.1016/j.ijdevneu.2015.09.004

Nagarkar-Jaiswal S, Deluca SZ, Lee PT, Lin WW, Pan H, Zuo Z, Lv J, Spradling AC, Bellen HJ. 2015a. A genetic toolkit for tagging intronic MiMIC containing genes. *Elife* **4**:2–9. doi:10.7554/eLife.08469

Nagarkar-Jaiswal S, Lee P-T, Campbell ME, Chen K, Anguiano-Zarate S, Cantu Gutierrez M, Busby T, Lin W-W, He Y, Schulze KL, Booth BW, Evans-Holm M, Venken KJ, Levis RW, Spradling AC, Hoskins R a, Bellen HJ. 2015b. A library of MiMICs allows tagging of genes and reversible, spatial and temporal knockdown of proteins in Drosophila. *Elife* **4**:1–28. doi:10.7554/eLife.05338

Nassif C, Noveen A, Hartenstein V. 2003. Early development of the Drosophila brain:

III. The pattern of neuropile founder tracts during the larval period. *J Comp Neurol* **455**:417–434. doi:10.1002/cne.10482

Ngo KT, Wang J, Junker M, Kriz S, Vo G, Asem B, Olson JM, Banerjee U, Hartenstein V. 2010. Concomitant requirement for Notch and Jak/Stat signaling during neuro-epithelial differentiation in the Drosophila optic lobe. *Dev Biol* **346**:284–295. doi:10.1016/j.ydbio.2010.07.036

Nwaobi SE, Cuddapah VA, Patterson KC, Randolph AC, Olsen ML. 2016. The role of glial-specific Kir4.1 in normal and pathological states of the CNS. *Acta Neuropathol* **132**:1–21. doi:10.1007/s00401-016-1553-1

Oatley MJ, Racicot KE, Oatley JM. 2011. Sertoli Cells Dictate Spermatogonial Stem Cell Niches in the Mouse Testis. *Biol Reprod* **84**:639–645. doi:10.1095/biolreprod.110.087320

Olsen ML, Khakh BS, Skatchkov SN, Zhou M, Lee CJ, Rouach N. 2015. New Insights on Astrocyte Ion Channels: Critical for Homeostasis and Neuron-Glia Signaling. *J Neurosci* **35**:13827–13835. doi:10.1523/JNEUROSCI.2603-15.2015

Orihara-Ono M, Toriya M, Nakao K, Okano H. 2011. Downregulation of Notch mediates the seamless transition of individual Drosophila neuroepithelial progenitors into optic medullar neuroblasts during prolonged G1. *Dev Biol* **351**:163–175. doi:10.1016/j.ydbio.2010.12.044

Pappalardo L, BLack J, Waxman SG. 2016. Sodium channels in astroglia and microglia. *Glia* **64**:1628–1645.

Pappu KS, Morey M, Nern A, Spitzweck B, Dickson BJ, Zipursky SL. 2011. Robo-3--mediated repulsive interactions guide R8 axons during Drosophila visual system development. *Proc Natl Acad Sci U S A* **108**:7571–7576.

Pereanu W, Shy D, Hartenstein V. 2005. Morphogenesis and proliferation of the larval

brain glia in Drosophila. *Dev Biol* **283**:191–203. doi:10.1016/j.ydbio.2005.04.024

Perez-Gomez R, Slovakova J, Rives-Quinto N, Krejci A, Carmena A. 2013. A Serrate-Notch-Canoe complex mediates essential interactions between glia and neuroepithelial cells during Drosophila optic lobe development. *J Cell Sci* **126**:4873–4884. doi:10.1242/jcs.125617

Perez SE, Steller H. 1996. Migration of glial cells into retinal axon target field in Drosophila melanogaster. *J Neurobiol* **30**:359–373.

Persi E, Duran-Frigola M, Damaghi M, Roush W, Aloy P, Cleveland J, Gillies R, Ruppin E. 2018. Systems analysis of intracellular pH vulnerabilities for cancer therapy. *Nat Commun* **9**:2997.

Plazaola-Sasieta H, Fernández-Pineda A, Zhu Q, Morey M. 2017. Untangling the wiring of the Drosophila visual system: developmental principles and molecular strategies. *J Neurogenet* **31**. doi:10.1080/01677063.2017.1391249

Poeck B, Fischer S, Gunning D, Zipursky SL, Salecker I. 2001. Glial cells mediate target layer selection of retinal axons in the developing visual system of Drosophila. *Neuron* **29**:99–113. doi:10.1016/S0896-6273(01)00183-0

Ratte S, Prescott SA. 2011. ClC-2 Channels Regulate Neuronal Excitability, Not Intracellular Chloride Levels. *J Neurosci* **31**:15838–15843. doi:10.1523/JNEUROSCI.2748-11.2011

Read RD. 2018. Pvr receptor tyrosine kinase signaling promotes post-embryonic morphogenesis and survival of glia and neural progenitor cells in *Drosophila*. *Development* dev.164285. doi:10.1242/dev.164285

Reddy BVVG, Rauskolb C, Irvine KD. 2010. Influence of Fat-Hippo and Notch signaling on the proliferation and differentiation of Drosophila optic neuroepithelia. *Development* **137**:2397–2408. doi:10.1242/dev.050013

Reillo I, De Juan Romero C, García-Cabezas MÁ, Borrell V. 2011. A Role for intermediate radial glia in the tangential expansion of the mammalian cerebral cortex. *Cereb Cortex* **21**:1674–1694. doi:10.1093/cercor/bhq238

Ren Q, Awasaki T, Wang Y-C, Huang Y-F, Lee T. 2018. Lineage-guided Notch-dependent gliogenesis by *Drosophila* multi-potent progenitors. *Development* **145**:dev160127. doi:10.1242/dev.160127

Rinke I, Artmann J, Stein V. 2010. ClC-2 Voltage-Gated Channels Constitute Part of the Background Conductance and Assist Chloride Extrusion. *J Neurosci* **30**:4776–4786. doi:10.1523/JNEUROSCI.6299-09.2010

Rose U, Derst C, Wanischeck M, Marinc C, Walther C. 2007. Properties and possible function of a hyperpolarisation-activated chloride current in Drosophila. *J Exp Biol* **210**:2489–2500. doi:10.1242/jeb.006361

Ruddy RM, Morshead CM. 2018. Home sweet home: the neural stem cell niche throughout development and after injury. *Cell Tissue Res* **371**:125–141. doi:10.1007/s00441-017-2658-0

Scholl UI, Choi M, Liu T, Ramaekers VT, Hausler MG, Grimmer J, Tobe SW, Farhi A, Nelson-Williams C, Lifton RP. 2009. Seizures, sensorineural deafness, ataxia, mental retardation, and electrolyte imbalance (SeSAME syndrome) caused by mutations in KCNJ10. *Proc Natl Acad Sci* **106**:5842–5847. doi:10.1073/pnas.0901749106

Shigetomi E, Patel S, Khakh BS. 2016. Probing the Complexities of Astrocyte Calcium Signaling. *Trends Cell Biol* **26**:300–312. doi:10.1016/j.tcb.2016.01.003

Sicca F, Ambrosini E, Marchese M, Sforna L, Servettini I, Valvo G, Brignone MS, Lanciotti A, Moro F, Grottesi A, Catacuzzeno L, Baldini S, Hasan S, D'adamo MC, Franciolini F, Molinari P, Santorelli FM, Pessia M. 2016. Gain-of-function

defects of astrocytic Kir4.1 channels in children with autism spectrum disorders and epilepsy. *Sci Rep* **6**:1–15. doi:10.1038/srep34325

Sicca F, Imbrici P, D'Adamo MC, Moro F, Bonatti F, Brovedani P, Grottesi A, Guerrini R, Masi G, Santorelli FM, Pessia M. 2011. Autism with Seizures and Intellectual Disability: Possible Causative Role of Gain-of-function of the Inwardly-Rectifying K+Channel Kir4.1. *Neurobiol Dis* **43**:239–247. doi:10.1016/j.nbd.2011.03.016

Sirisi S, Elorza-Vidal X, Arnedo T, Armand-Ugón M, Callejo G, Capdevila-Nortes X, López-Hernández T, Schulte U, Barrallo-Gimeno A, Nunes V, Gasull X, Estévez R. 2017. Depolarization causes the formation of a ternary complex between GlialCAM, MLC1 and ClC-2 in astrocytes: implications in megalencephalic leukoencephalopathy. *Hum Mol Genet* **26**:2436–2450. doi:10.1093/hmg/ddx134

Smith RS, Kenny CJ, Ganesh V, Jang A, Borges-Monroy R, Partlow JN, Hill RS, Shin T, Chen AY, Doan RN, Anttonen A-K, Ignatius J, Medne L, Bönnemann CG, Hecht JL, Salonen O, Barkovich AJ, Poduri A, Wilke M, de Wit MCY, Mancini GMS, Sztriha L, Im K, Amrom D, Andermann E, Paetau R, Lehesjoki A-E, Walsh CA, Lehtinen MK. 2018. Sodium Channel SCN3A (NaV1.3) Regulation of Human Cerebral Cortical Folding and Oral Motor Development. *Neuron* **99**:905–913.e7. doi:10.1016/j.neuron.2018.07.052

Sousa-Nunes R, Yee LL, Gould AP. 2011. Fat cells reactivate quiescent neuroblasts via TOR and glial insulin relays in Drosophila. *Nature* **471**:508–513. doi:10.1038/nature09867

Spéder P, Brand AH. 2018. Systemic and local cues drive neural stem cell niche remodelling during neurogenesis in drosophila. *Elife* **7**:1–16. doi:10.7554/eLife.30413

Spéder P, Brand AH. 2014. Gap junction proteins in the blood-brain barrier control

nutrient-dependent reactivation of Drosophila neural stem cells. *Dev Cell* **30**:309–321. doi:10.1016/j.devcel.2014.05.021

Spindler SR, Ortiz I, Fung S, Takashima S, Hartenstein V. 2009. Drosophila cortex and neuropile glia influence secondary axon tract growth, pathfinding, and fasciculation in the developing larval brain. *Dev Biol* **334**:355–368. doi:10.1016/j.ydbio.2009.07.035

Stork T, Sheehan A, Tasdemir-Yilmaz OE, Freeman MR. 2014. Neuron-Glia interactions through the heartless fgf receptor signaling pathway mediate morphogenesis of drosophila astrocytes. *Neuron* **83**:388–403. doi:10.1016/j.neuron.2014.06.026

Suzuki T, Hasegawa E, Nakai Y, Kaido M, Takayama R, Sato M. 2016. Formation of Neuronal Circuits by Interactions between Neuronal Populations Derived from Different Origins in the Drosophila Visual Center. *Cell Rep* **15**:499–509. doi:10.1016/j.celrep.2016.03.056

Tayler T, Robixaux M, Garrity P. 2004. Compartmentalization of visual centers in the Drosophila brain requires Slit and Robo proteins. *Development* **131**:5935–5945. doi:10.1242/dev.01465

Tomancak P, Beaton A, Weiszmann R, Kwan E, Shu S, Lewis SE, Richards S, Ashburner M, Hartenstein V, Celniker SE, Rubin GM. 2002. Systematic determination of patterns of gene expression during Drosophila embryogenesis. *Genome Biol* **3**:RESEARCH0088.

Tomancak P, Berman BP, Beaton A, Weiszmann R, Kwan E, Hartenstein V, Celniker SE, Rubin GM. 2007. Global analysis of patterns of gene expression during Drosophila embryogenesis. *Genome Biol* **8**:1–24. doi:10.1186/gb-2007-8-7-r145

Ugarte G, Delgado R, O'Day PM, Farjah F, Cid LP, Vergara C, Bacigalupo J. 2005.

Putative ClC-2 chloride channel mediates inward rectification in Drosophila retinal photoreceptors. *J Membr Biol* **207**:151–160. doi:10.1007/s00232-005-0810-3

Venken KJT, Schulze KL, Haelterman NA, Pan H, He Y, Evans-Holm M, Carlson JW, Levis RW, Spradling AC, Hoskins RA, Bellen HJ. 2011. MiMIC: a highly versatile transposon insertion resource for engineering Drosophila melanogaster genes. *Nat Methods* **8**:737–743.

Verkhrastsky A, Steinhauser C. 2000. Ion channels in glial cells. *Brain Res* **32**:380–412.

Viktorin G, Riebli N, Reichert H. 2013. A multipotent transit-amplifying neuroblast lineage in the central brain gives rise to optic lobe glial cells in Drosophila. *Dev Biol* **379**:182–194. doi:10.1016/j.ydbio.2013.04.020

Wang H, Xu M, Kong Q, Sun P, Yan F, Tian W, Wang X. 2017. Research and progress on ClC-2 (Review). *Mol Med Rep* **16**:11–22. doi:10.3892/mmr.2017.6600

Wang JW, Beck ES, McCabe BD. 2012. A modular toolset for recombination transgenesis and neurogenetic analysis of Drosophila. *PLoS One* **7**. doi:10.1371/journal.pone.0042102

Wang W, Li Y, Zhou L, Yue H, Luo H. 2011a. Role of JAK/STAT signaling in neuroepithelial stem cell maintenance and proliferation in the Drosophila optic lobe. *Biochem Biophys Res Commun* **410**:714–720. doi:10.1016/j.bbrc.2011.05.119

Wang W, Liu W, Wang Y, Zhou L, Tang X, Luo H. 2011b. Notch signaling regulates neuroepithelial stem cell maintenance and neuroblast formation in Drosophila optic lobe development. *Dev Biol* **350**:414–428.

Weng M, Haenfler JM, Lee CY. 2012. Changes in Notch signaling coordinates maintenance and differentiation of the Drosophila larval optic lobe neuroepithelia. *Dev Neurobiol* **72**:1376–1390. doi:10.1002/dneu.20995

White KA, Grillo-Hill BK, Barber DL. 2017. Cancer cell behaviors mediated by dysregulated pH dynamics at a glance. *J Cell Sci* **130**:663–669. doi:10.1242/jcs.195297

Yasugi T, Sugie A, Umetsu D, Tabata T. 2010. Coordinated sequential action of EGFR and Notch signaling pathways regulates proneural wave progression in the Drosophila optic lobe. *Development* **137**:3193–3203. doi:10.1242/dev.048058

Yasugi T, Umetsu D, Murakami S, Sato M, Tabata T. 2008. Drosophila optic lobe neuroblasts triggered by a wave of proneural gene expression that is negatively regulated by JAK/STAT. *Development* **135**:1471–1480. doi:10.1242/dev.019117

Zhu CC, Boone JQ, Jensen PA, Hanna S, Podemski L, Locke J, Doe CQ, O'Connor MB. 2008. Drosophila Activin- and the Activin-like product Dawdle function redundantly to regulate proliferation in the larval brain. *Development* **135**:513–521. doi:10.1242/dev.010876

Figure 1

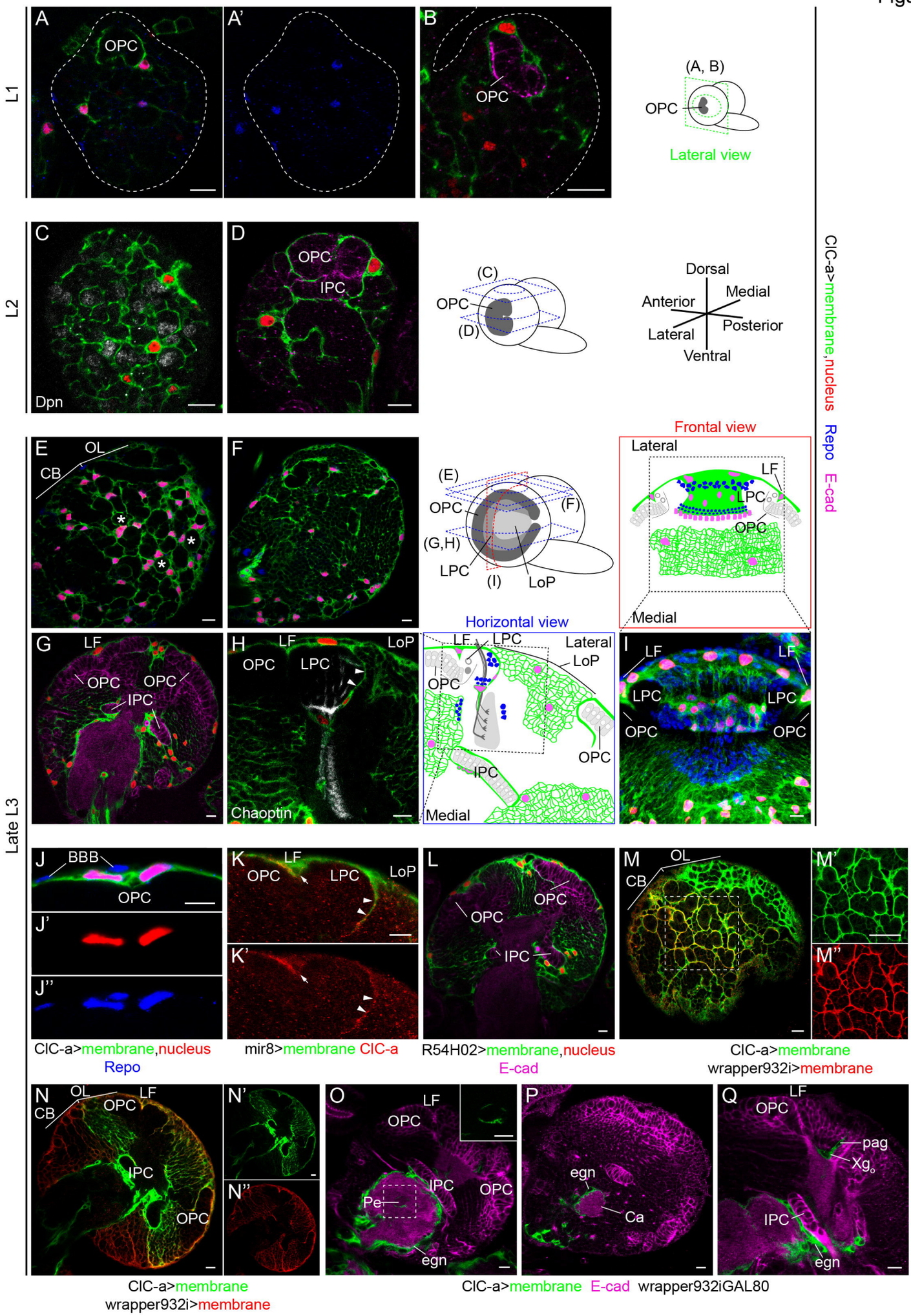
L1
L2
Late L3
A
A'
B
OPC
(A, B)
Lateral view
C
D
Dpn
IPC
(C)
(D)
Dorsal
Medial
Anterior
Posterior
Lateral
Ventral
E
F
OL
CB
(E)
(F)
(G,H)
(I)
LPC
LoP
Frontal view
Lateral
Medial
G
H
I
LF
Chaoptin
Horizontal view
J
J'
J''
BBB
K
K'
L
M
M'
M''
CB
ClC-a>membrane,nucleus
Repo
mir8>membrane ClC-a
R54H02>membrane,nucleus
E-cad
ClC-a>membrane
wrapper932i>membrane
N
N'
N''
O
P
Q
egn
Ca
Pe
pag
Xg
ClC-a>membrane
wrapper932i>membrane
ClC-a>membrane E-cad wrapper932iGAL80
ClC-a>membrane,nucleus Repo E-cad

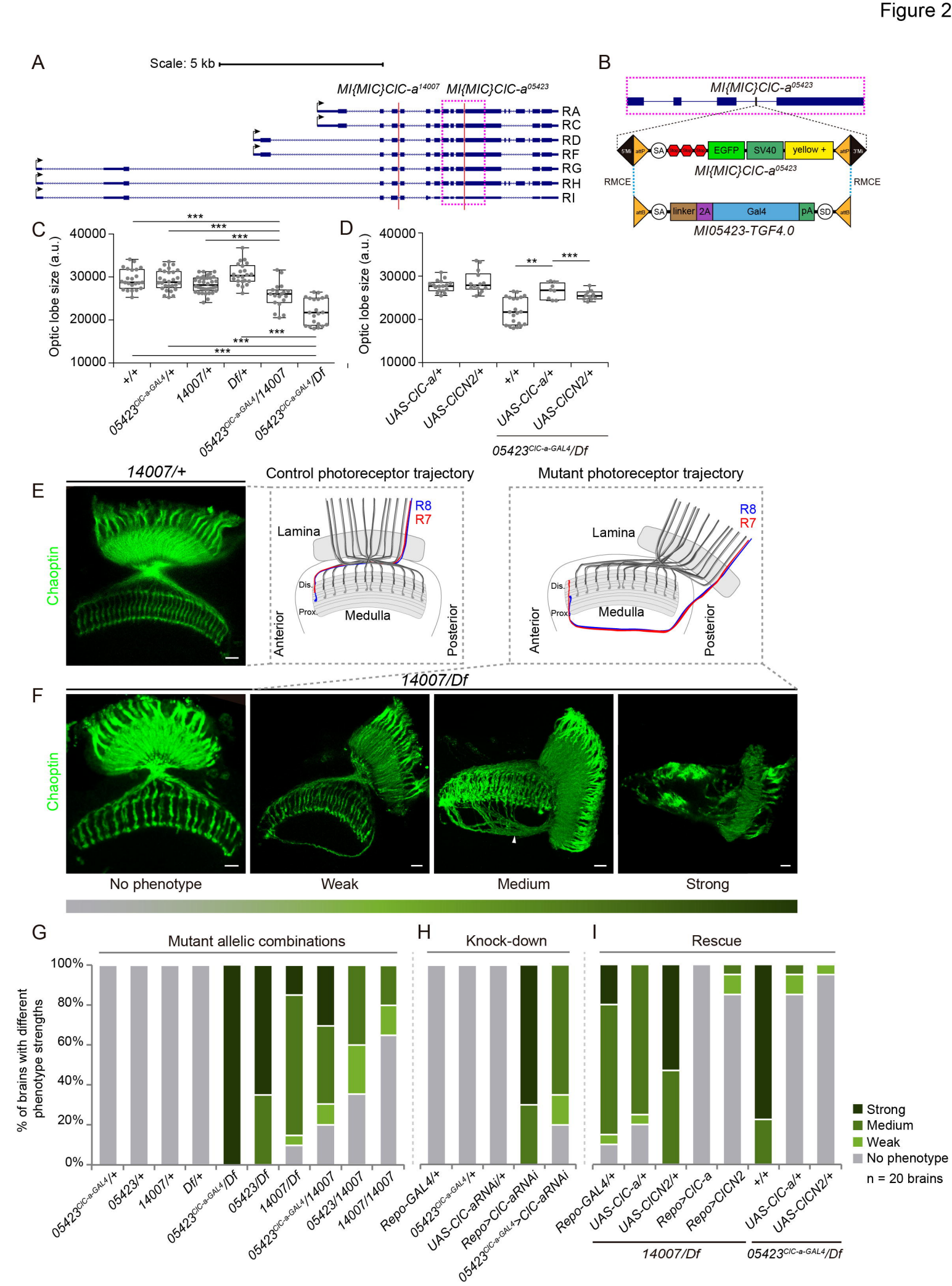
A
Scale: 5 kb
MI{MIC}ClC-a14007
MI{MIC}ClC-a05423
RA
RC
RD
RF
RG
RH
RI
B
MI{MIC}ClC-a05423
EGFP
SV40
yellow +
SA
RMCE
RMCE
MI{MIC}ClC-a05423
linker
2A
Gal4
pA
SD
MI05423-TGF4.0
C
Optic lobe size (a.u.)
40000
30000
20000
10000
+/+
05423ClC-a-GAL4/+
14007/+
Df/+
05423ClC-a-GAL4/14007
05423ClC-a-GAL4/Df
D
Optic lobe size (a.u.)
UAS-ClC-a/+
UAS-ClCN2/+
+/+
UAS-ClC-a/+
UAS-ClCN2/+
05423ClC-a-GAL4/Df
E
14007/+
Chaoptin
Control photoreceptor trajectory
Mutant photoreceptor trajectory
Lamina
R8
R7
Dis.
Prox.
Medulla
Anterior
Posterior
F
14007/Df
Chaoptin
No phenotype
Weak
Medium
Strong
G
Mutant allelic combinations
% of brains with different phenotype strengths
100%
80%
60%
40%
20%
0%
05423ClC-a-GAL4/+
05423/+
14007/+
Df/+
05423ClC-a-GAL4/Df
05423/Df
14007/Df
05423ClC-a-GAL4/14007
05423/14007
14007/14007
H
Knock-down
Repo-GAL4/+
05423ClC-a-GAL4/+
UAS-ClC-aRNAi/+
Repo>ClC-aRNAi
05423ClC-a-GAL4>ClC-aRNAi
I
Rescue
Repo-GAL4/+
UAS-ClC-a/+
UAS-ClCN2/+
Repo>ClC-a
Repo>ClCN2
+/+
UAS-ClC-a/+
UAS-ClCN2/+
14007/Df
05423ClC-a-GAL4/Df
Strong
Medium
Weak
No phenotype
n = 20 brains

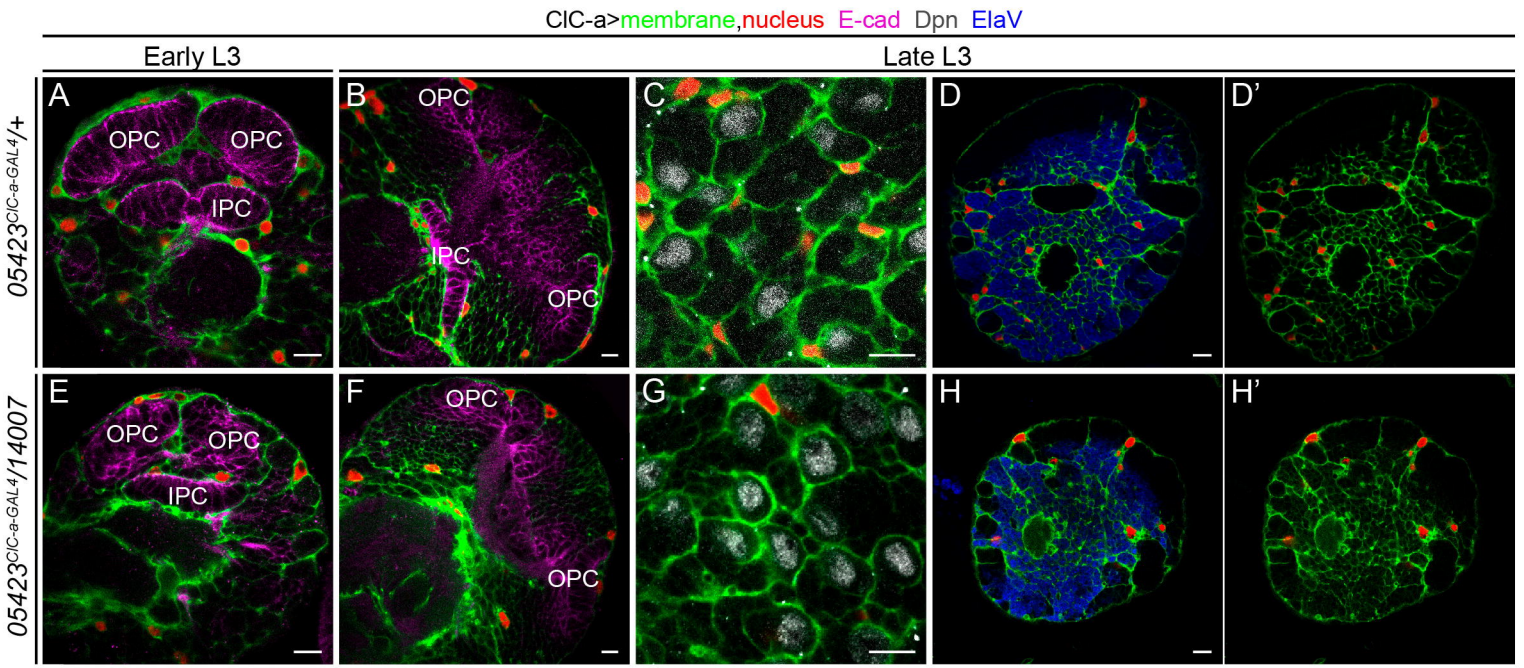
ClC-a>membrane,nucleus E-cad Dpn ElaV
Early L3
Late L3
05423ClC-a-GAL4/+
05423ClC-a-GAL4/14007
A
B
C
D
D'
E
F
G
H
H'
OPC
IPC

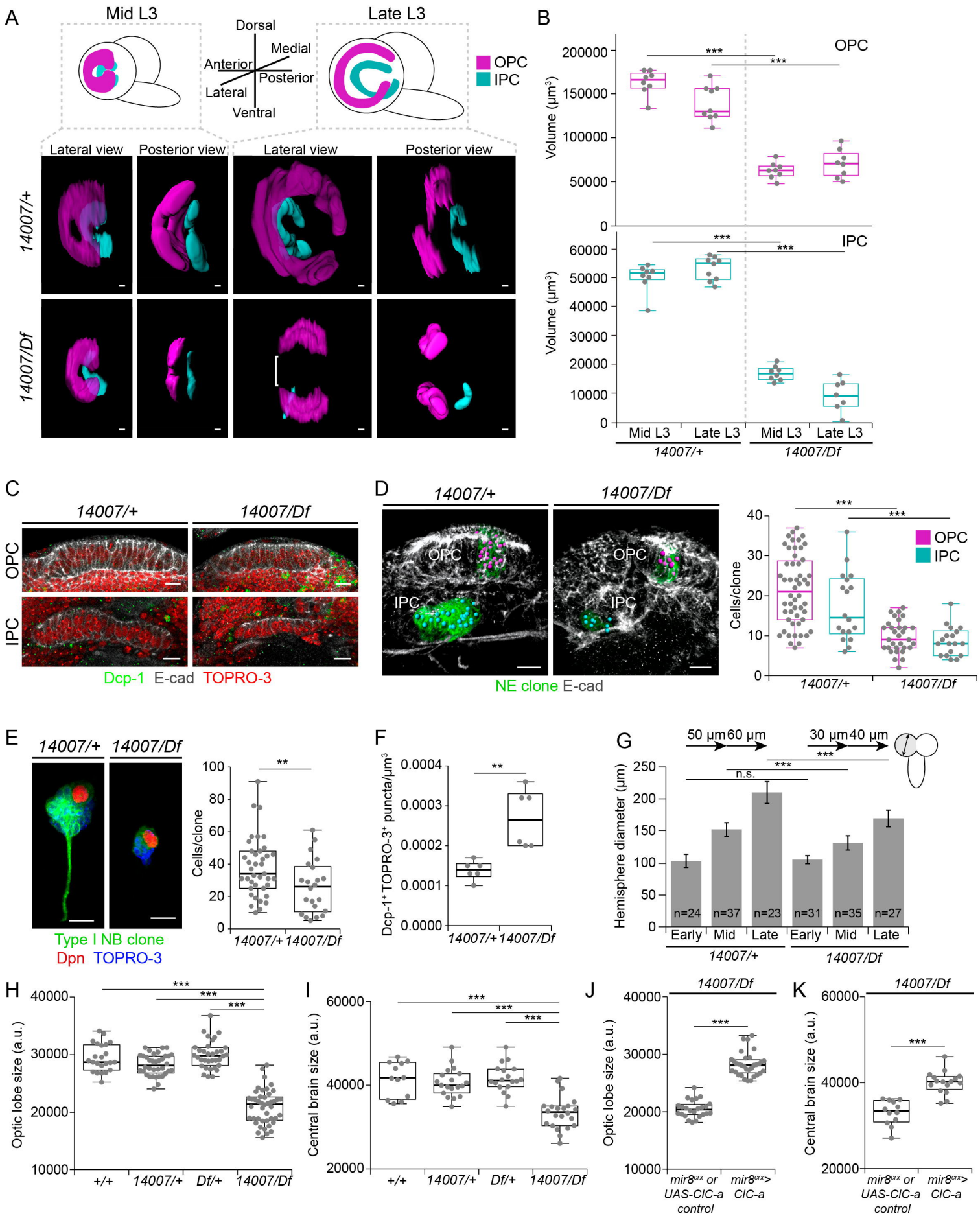
A
Mid L3
Late L3
Dorsal
Medial
Anterior
Posterior
Lateral
Ventral
OPC
IPC
Lateral view
Posterior view
Lateral view
Posterior view
14007/+
14007/Df
B
OPC
IPC
Volume (μm³)
Mid L3
Late L3
Mid L3
Late L3
14007/+
14007/Df
C
14007/+
14007/Df
OPC
IPC
Dcp-1 E-cad TOPRO-3
D
14007/+
14007/Df
OPC
IPC
NE clone E-cad
Cells/clone
14007/+
14007/Df
E
14007/+ 14007/Df
Type I NB clone
Dpn TOPRO-3
Cells/clone
14007/+ 14007/Df
F
Dcp-1⁺ TOPRO-3⁺ puncta/μm³
14007/+ 14007/Df
G
50 μm 60 μm
30 μm 40 μm
n.s.
Hemisphere diameter (μm)
n=24
n=37
n=23
n=31
n=35
n=27
Early
Mid
Late
Early
Mid
Late
14007/+
14007/Df
H
Optic lobe size (a.u.)
+/+
14007/+
Df/+
14007/Df
I
Central brain size (a.u.)
+/+
14007/+
Df/+
14007/Df
J
14007/Df
Optic lobe size (a.u.)
mir8crx or UAS-ClC-a control
mir8crx> ClC-a
K
14007/Df
Central brain size (a.u.)
mir8crx or UAS-ClC-a control
mir8crx> ClC-a

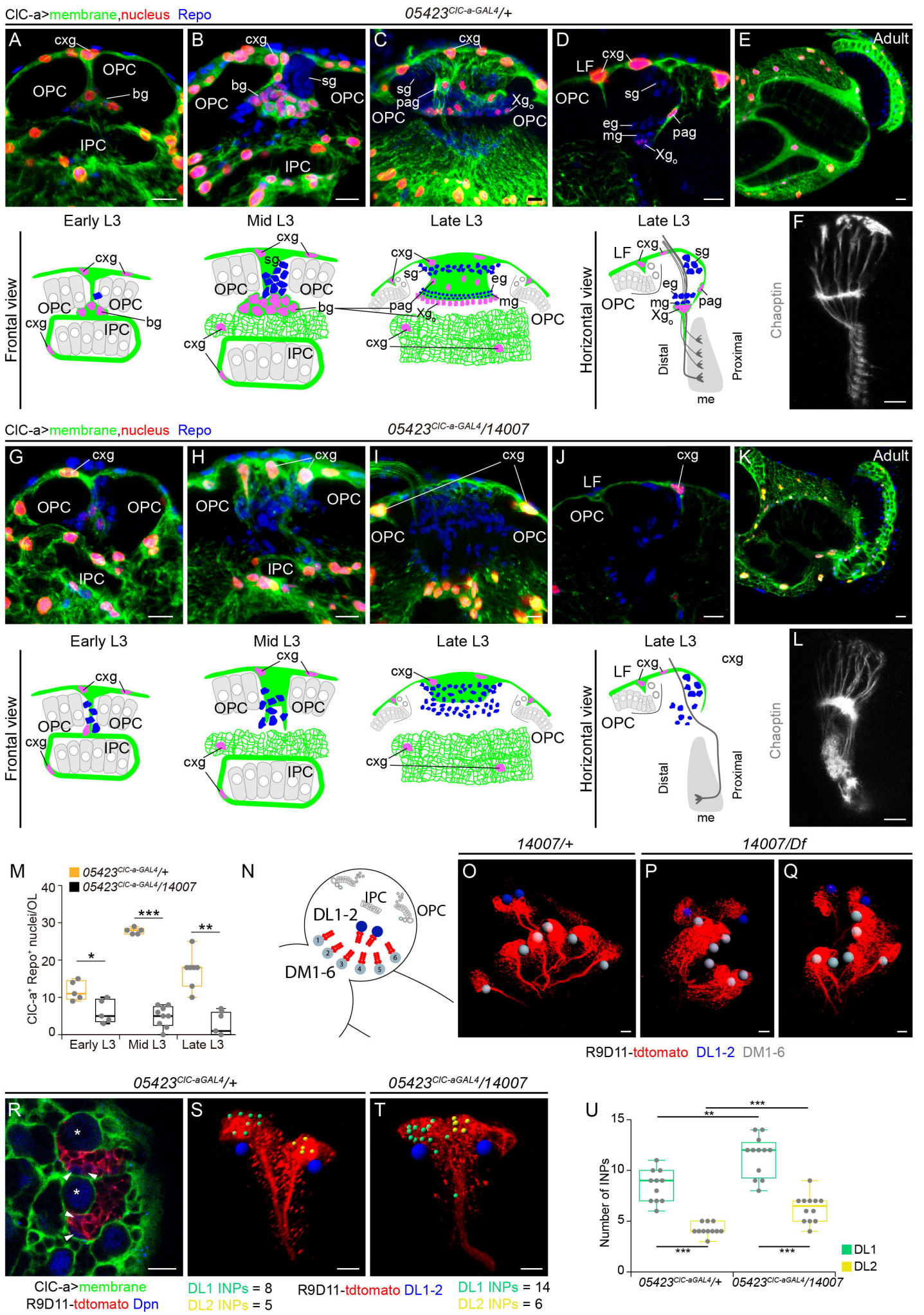
ClC-a>membrane,nucleus Repo
05423ClC-a-GAL4/+
A
B
C
D
E
Adult
cxg
OPC
bg
sg
IPC
pag
Xgo
LF
eg
mg
Early L3
Mid L3
Late L3
Frontal view
Horizontal view
Distal
Proximal
me
F
Chaoptin
ClC-a>membrane,nucleus Repo
05423ClC-a-GAL4/14007
G
H
I
J
K
L
M
05423ClC-a-GAL4/+
05423ClC-a-GAL4/14007
ClC-a+ Repo+ nuclei/OL
N
DL1-2
DM1-6
14007/+
14007/Df
O
P
Q
R9D11-tdtomato DL1-2 DM1-6
R
S
T
ClC-a>membrane
R9D11-tdtomato Dpn
DL1 INPs = 8
DL2 INPs = 5
R9D11-tdtomato DL1-2
DL1 INPs = 14
DL2 INPs = 6
U
Number of INPs
DL1
DL2

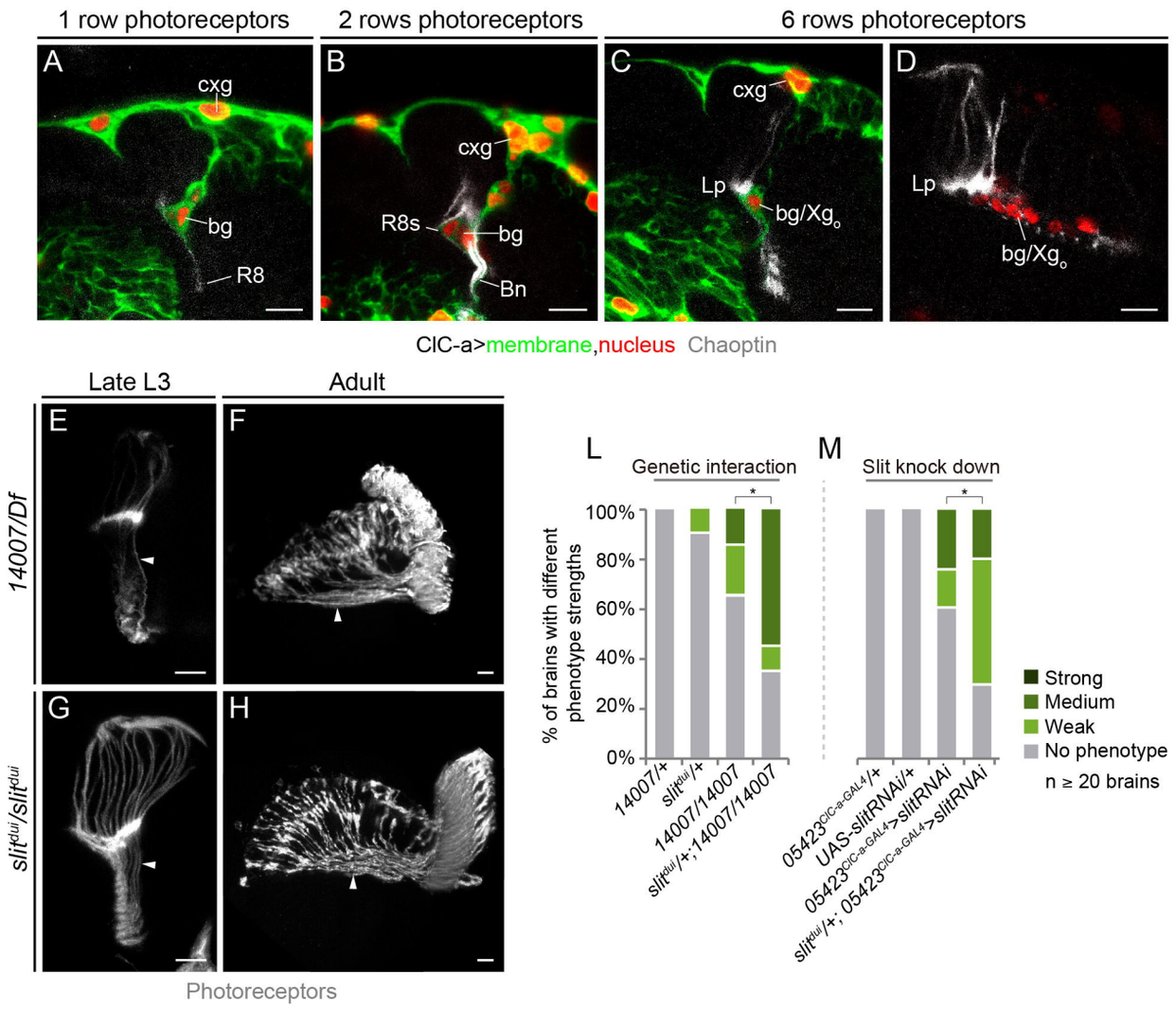
1 row photoreceptors
2 rows photoreceptors
6 rows photoreceptors
A
B
C
D
cxg
bg
R8
R8s
Bn
Lp
bg/Xg$_o$
ClC-a>membrane,nucleus Chaoptin
Late L3
Adult
E
F
G
H
14007/Df
slit^{dui}/slit^{dui}
Photoreceptors
L
Genetic interaction
M
Slit knock down
% of brains with different phenotype strengths
100%
80%
60%
40%
20%
0%
14007/+
slit^{dui}/+
14007/14007
slit^{dui}/+;14007/14007
05423$^{ClC-a-GAL4}$/+
UAS-slitRNAi/+
05423$^{ClC-a-GAL4}$>slitRNAi
slit^{dui}/+; 05423$^{ClC-a-GAL4}$>slitRNAi
Strong
Medium
Weak
No phenotype
n ≥ 20 brains

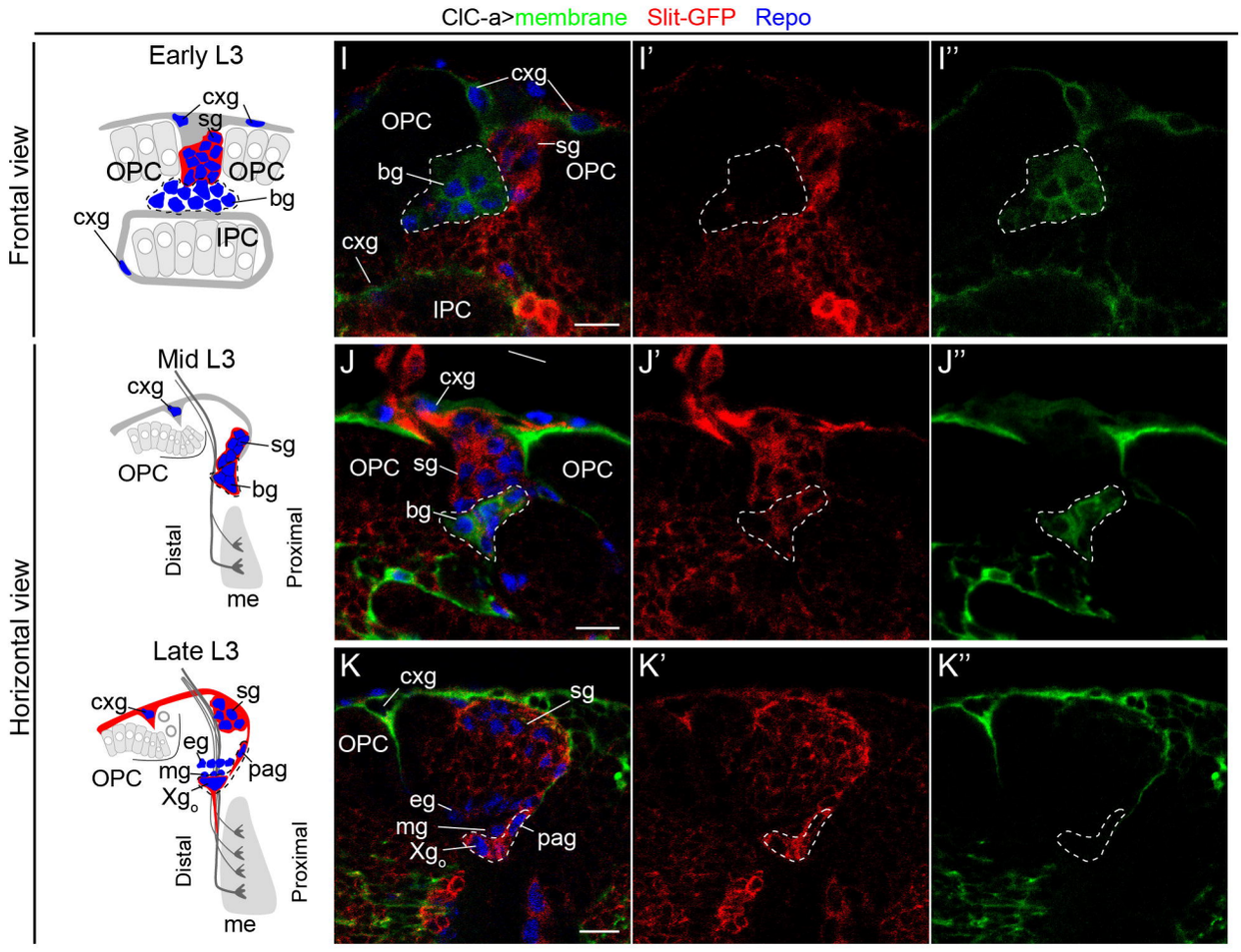
ClC-a>membrane Slit-GFP Repo
Frontal view
Horizontal view
Early L3
Mid L3
Late L3
cxg
sg
OPC
bg
IPC
eg
mg
pag
Xg$_o$
Distal
Proximal
me
I
I'
I''
J
J'
J''
K
K'
K''

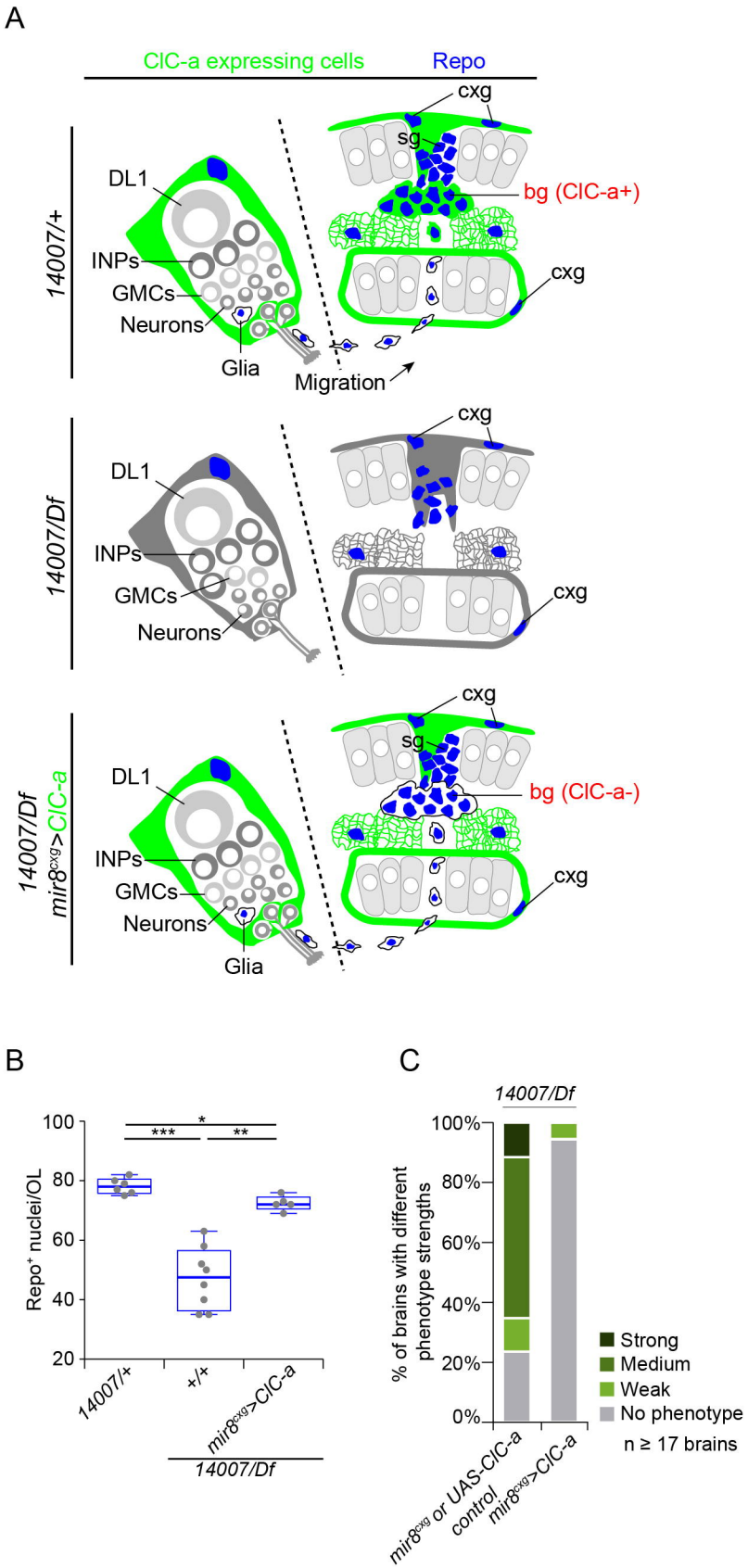
A
ClC-a expressing cells
Repo
14007/+
DL1
INPs
GMCs
Neurons
Glia
cxg
sg
bg (ClC-a+)
Migration
14007/Df
bg (ClC-a-)
mir8cxg>ClC-a
B
Repo+ nuclei/OL
100
80
60
40
20
*
***
**
14007/+
+/+
mir8cxg>ClC-a
14007/Df
C
14007/Df
% of brains with different phenotype strengths
100%
80%
60%
40%
20%
0%
Strong
Medium
Weak
No phenotype
n ≥ 17 brains
mir8cxg or UAS-ClC-a control
mir8cxg>ClC-a

Figure 8

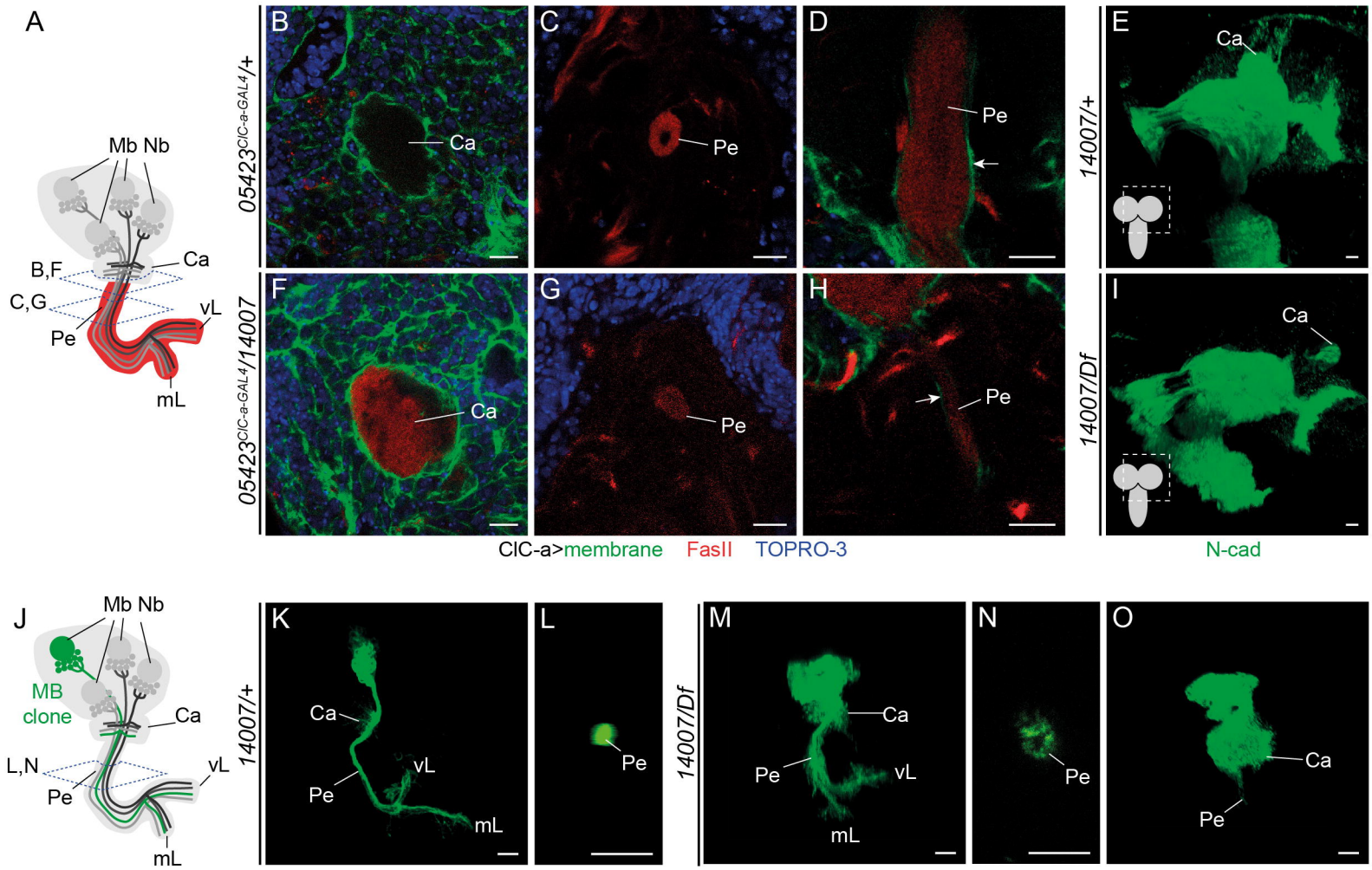
A
Mb Nb
B,F
Ca
C,G
vL
Pe
mL
05423ClC-a-GAL4/+
05423ClC-a-GAL4/14007
B
C
D
E
F
G
H
I
Ca
Pe
14007/+
14007/Df
ClC-a>membrane
FasII
TOPRO-3
N-cad
J
MB clone
L,N
K
L
M
N
O